iScience

CellPress
OPEN ACCESS

Article

ΔNp63 regulates MDSC survival and metabolism in triple-negative breast cancer

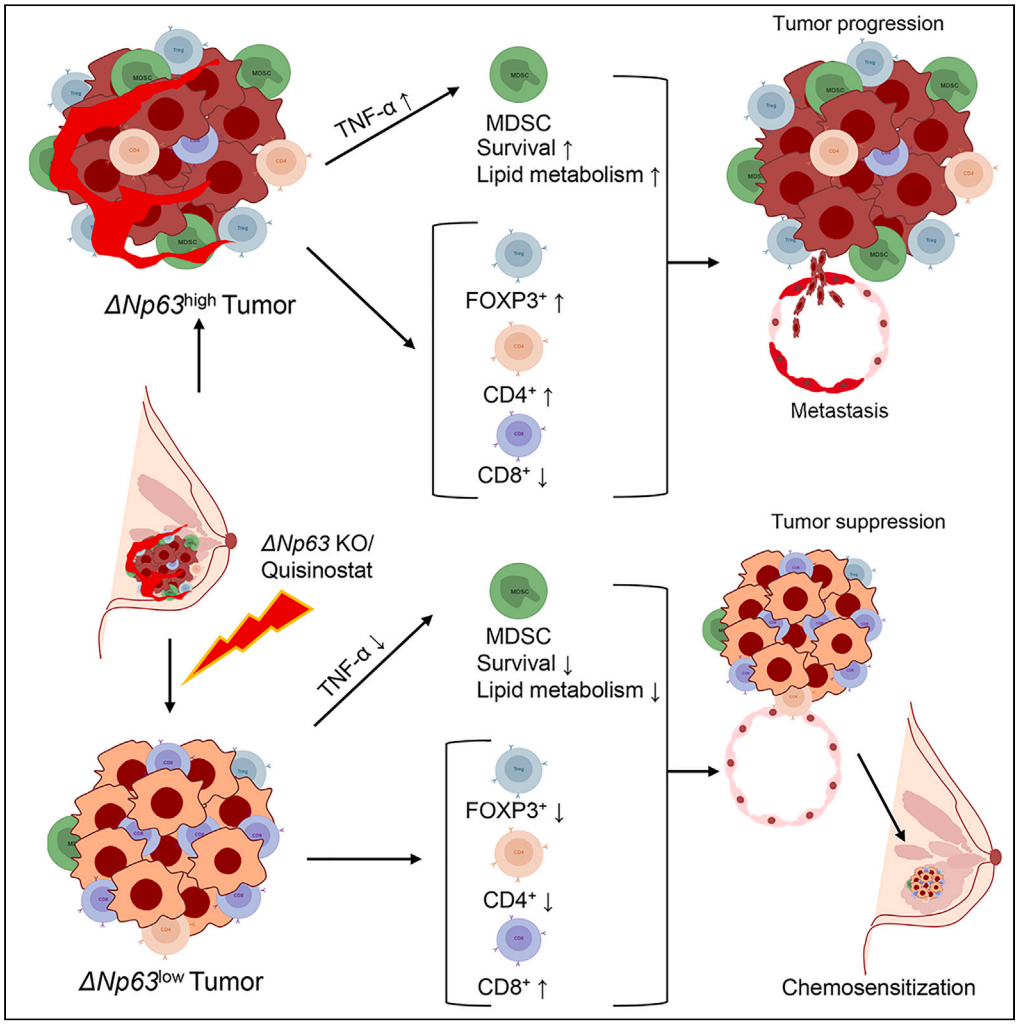

Ukjin Kim, Rahul Debnath, Javier E. Maiz, Joshua Rico, Satrajit Sinha, Mario Andrés Blanco, Rumela Chakrabarti

rxc1335@med.miami.edu

Highlights

Loss of *ΔNp63* reduces progression and metastasis in advanced TNBC via MDSC survival

ΔNp63 levels in tumor cells regulate survival of MDSCs through TNF-α

ΔNp63 regulates multiple metabolic properties of MDSC including lipid metabolism

Targeting ΔNp63 using new HDACi, Quisinostat, sensitizes TNBC to chemotherapy

Kim et al., iScience 27, 109366
April 19, 2024
https://doi.org/10.1016/j.isci.2024.109366

iScience

CellPress
OPEN ACCESS

Article

ΔNp63 regulates MDSC survival and metabolism in triple-negative breast cancer

Ukjin Kim,[1,4] Rahul Debnath,[2,4] Javier E. Maiz,[1] Joshua Rico,[2] Satrajit Sinha,[3] Mario Andrés Blanco,[2] and Rumela Chakrabarti[1,2,5,*]

SUMMARY

Triple-negative breast cancer (TNBC) contributes greatly to mortality of breast cancer, demanding new targetable options. We have shown that TNBC patients have high *ΔNp63* expression in tumors. However, the function of ΔNp63 in established TNBC is yet to be explored. In current studies, targeting ΔNp63 with inducible CRISPR knockout and Histone deacetylase inhibitor Quisinostat showed that ΔNp63 is important for tumor progression and metastasis in established tumors by promoting myeloid-derived suppressor cell (MDSC) survival through tumor necrosis factor alpha. Decreasing ΔNp63 levels are associated with decreased $CD4^+$ and $FOXP3^+$ T-cells but increased $CD8^+$ T-cells. RNA sequencing analysis indicates that loss of ΔNp63 alters multiple MDSC properties such as lipid metabolism, chemotaxis, migration, and neutrophil degranulation besides survival. We further demonstrated that targeting ΔNp63 sensitizes chemotherapy. Overall, we showed that ΔNp63 reprograms the MDSC-mediated immunosuppressive functions in TNBC, highlighting the benefit of targeting ΔNp63 in chemotherapy-resistant TNBC.

INTRODUCTION

Breast cancer can be divided into molecular subtypes according to receptor expression. Estrogen receptor-negative, progesterone receptor-negative, and HER2-negative triple-negative breast cancer (TNBC) accounts for 15%–20% of all breast cancers.[1] TNBC rarely responds to hormonal therapy or anti-HER2 therapy because the receptor does not exist, contributing greatly to mortality in breast cancer. The main treatment for TNBC is conventional cytotoxic systemic chemotherapy.[2] Doxorubicin is one of the most commonly used systemic chemotherapeutic agents.[3] However, it is well recognized that TNBC usually acquires resistance to doxorubicin leading to a multiple-drug resistance phenotype.[4] Less than 30% of TNBC patients can achieve a complete response with chemotherapy,[5] and more than 50% experience a relapse 3 to 5 years after initial diagnosis.[6] Considering drug resistance, strategies of multiple targeted therapeutics and combination of regimens are essential to effectively treat TNBC.

Transformation-related protein 63 (Trp63 or p63) is a transcription factor belonging to the p53/p63/p73 family and is highly expressed in breast epithelial cells.[7,8] p63 is divided into two isoforms: TAp63 with a transactivation domain and ΔNp63 without the domain.[9] Unlike TAp63, which has a tumor-suppressive function,[10,11] ΔNp63 has been reported to have an oncogenic function in cancers including head and neck squamous cell carcinoma,[12–14] prostate,[15] and breast cancers.[16–18] We reported earlier that ΔNp63 activates stem cell activity through Wnt signaling in TNBC and leads to tumor initiation.[17] We have also shown that human TNBC patients have higher levels of ΔNp63 expression than non-TNBC patients, and that ΔNp63-high tumors cause recruitment of myeloid-derived immune suppressor cells (MDSCs) in initiation stages of tumor development.[16] However, the function of ΔNp63 in advanced and metastatic TNBC is not yet studied. Additionally, the relationship of ΔNp63 with immune cells in advanced tumors remains unexplored.

In pathological environments such as cancer, immature myeloid cells are inclined toward differentiation into MDSCs, creating an immunosuppressive microenvironment in which cancer can benefit from immune evasion.[19,20] MDSCs are involved in the differentiation and expansion of $FOXP3^+$ regulatory T-cells[21,22] and interact with tumor-associated macrophages (TAMs) and dendritic cells (DCs) to promote tumor-induced immune suppression.[23] MDSCs also help immune evasion of cancer cells by inhibiting T cell activation and proliferation.[24] Although we have shown that recruitment of MDSCs by $\Delta Np63^+$ tumors promotes TNBC proliferation and metastasis in the initiation stage of tumors,[16] it is still unknown what effect ΔNp63 inhibition has on the immune cell population, particularly on MDSC survival, metabolism, and reprogramming in therapy-resistant advanced TNBC. Since TNBC patients in clinic already have established tumors, understanding the function of ΔNp63 and its associated immune cells such as MDSCs will be of high clinical impact, as it will help to design new drug targets for advanced

[1]Department of Surgery, Sylvester Comprehensive Cancer, University of Miami Miller School of Medicine, Miami, FL 33136, USA
[2]Department of Biomedical Sciences, School of Veterinary Medicine, University of Pennsylvania, Philadelphia, PA 19104, USA
[3]Department of Biochemistry, Jacobs School of Medicine and Biomedical Sciences, State University of New York at Buffalo, Buffalo, NY 14203, USA
[4]These authors contributed equally
[5]Lead contact
*Correspondence: rxc1335@med.miami.edu
https://doi.org/10.1016/j.isci.2024.109366

TNBC patients. Moreover, since chemotherapy fails a large number of advanced TNBC patients, finding new ways to sensitize chemotherapy response in TNBC patients is of paramount interest in the field.

In this study, we demonstrate that ΔNp63 is important for tumor progression and metastasis using a genetically engineered mouse model (GEMM) MMTV-Wnt1 and multiple inducible syngeneic TNBC allografts. Targeting ΔNp63 by an histone deacetylase (HDAC) inhibitor in established TNBC reduces tumor progression and metastasis. Targeting ΔNp63 also inhibits MDSC survival through cytokine tumor necrosis factor alpha (TNF-α), remodeling the tumor microenvironment with altered $CD4^+$, $FOXP3^+$, and $CD8^+$ T-cells. Furthermore, we show that targeting ΔNp63 sensitizes TNBC to chemotherapy. We propose that ΔNp63 is a potential target for chemotherapy-resistant TNBC patients through its action on MDSCs.

RESULTS

Conditional loss of ΔNp63 reduces MDSC survival and tumor progression in established spontaneous MMTV-Wnt1 basal/TNBC tumors

To understand ΔNp63 inhibition in developed TNBC, we employed MMTV-Wnt1 mice,[25] which have higher expression of *ΔNp63*, predominant isoform of p63,[17] and represent basal TNBC.[26] MMTV-Wnt1 mice that spontaneously develop TNBC were mated with mice carrying tamoxifen-inducible *K14-Cre*[27,28] and *ΔNp63*$^{f/f}$[29,30] to obtain *MMTV-Wnt1;iK14-Cre;ΔNp63*$^{f/f}$ mice. We compared tumor growth in *ΔNp63* wild-type (WT; *iK14-Cre*$^-$, *ΔNp63*$^{f/f}$ or *iK14-Cre*$^+$, *ΔNp63*$^{f/f}$, vehicle control for tamoxifen added) Wnt1 mice and *ΔNp63* inducible conditional KO (icKO) (*iK14-Cre*$^+$, *ΔNp63*$^{f/f}$ with tamoxifen) Wnt1 mice, when the tumors reached about average of 500 mm^3. Results showed that tumor growth was immediately inhibited in *ΔNp63* icKO mice, suggesting that targeting ΔNp63 is instantaneously effective in spontaneously developed tumors (Figure 1A). To evaluate the effect of ΔNp63 inhibition on metastasis, lymph nodes were stained with K14 and S100A8 (marker of MDSCs) antibodies to analyze metastasis and infiltration of MDSCs (Figure 1B). Immunostaining revealed that *ΔNp63* icKO mice showed decreased MDSC infiltration and reduced numbers of metastatic $K14^+$ basal tumor cells in lymph nodes, implying that targeting ΔNp63 can inhibit metastasis of spontaneous basal tumors with high ΔNp63, which is associated with reduced MDSC number (Figures 1C and 1D). Immunostaining for ΔNp63 showed that tamoxifen-inducible Cre successfully induced *ΔNp63* icKO, demonstrating that the reduced tumor growth and metastasis phenotype resulted from ΔNp63 loss (Figures 1E and 1F). To further elucidate the mechanism of decreased tumor progression by *ΔNp63* icKO, we evaluated the proliferative index Ki67 and apoptotic index cleaved caspase 3 (Ccl3). *ΔNp63* icKO tumors showed decreased Ki67 levels (Figures S1A and S1B) and increased Ccl3 (Figures S1C and S1D), implying loss of ΔNp63 resulted in decreased proliferation and increased cell death of tumor cells. To understand whether loss of ΔNp63 is accompanied by alterations in the immune landscape in the primary tumor, which is associated with tumor cell proliferation and survival, we investigated MDSC number, $CD4^+$, $FOXP3^+$, and $CD8^+$ T-cells, which are deeply associated with immune evasion.[31] *ΔNp63* icKO tumors were stained with S100A8 antibody, a marker of MDSCs, via immunofluorescence (IF) and showed a decrease in the number of MDSCs, suggesting that the suppression of tumor progression by *ΔNp63* icKO is potentially mediated by changes in MDSCs (Figures 1G and 1H). *ΔNp63* icKO tumors also showed a decreased number of $CD4^+$ T-cells (Figures 1I and 1J). In correlation with decreased $CD4^+$ T-cells, the significant decrease in $FOXP3^+$ regulatory T-cells suggested that the immune landscape had been remodeled from immune evasion to immune surveillance (Figures 1K and 1L). *ΔNp63* icKO tumors showed an increase in cytotoxic $CD8^+$ T-cells, which may be attributable to the decreased T cell suppression by MDSCs with ΔNp63 loss (Figures 1M and 1N). Similar to the IF results, flow cytometry showed a significant decrease in MDSCs in *ΔNp63* icKO tumors (Figure S1E). To understand if fewer MDSCs in *ΔNp63* icKO tumors were the result of increased cell death of MDSCs, we analyzed $Ccl3^+$ in MDSCs. We found by both co-immunofluorescence (co-IF) and fluorescence-activated cell sorting (FACS) analysis that $Ccl3^+$ MDSCs were higher in *ΔNp63* icKO tumors, suggesting that ΔNp63 plays an important role in MDSC survival (Figures 1O, 1P, S1F, and S1G). However, there was no significant change in the $Ccl3^+$ population among $EpCAM^+$ tumor cells, suggesting that the increase in $Ccl3^+$ cells found by immunohistochemistry (IHC) may be contributed mostly by MDSCs, not tumor cells (Figures S1H and S1I). We also analyzed the MDSC population in the blood to examine MDSC recruitment. $Ly6G^+$ polymorphonuclear-MDSCs (PMN-MDSCs) and $Ly6C^+$ monocytic-MDSCs (M-MDSCs) showed no differences between WT and *ΔNp63* icKO tumor-bearing mice (Figures S1J and S1K). However, $Ly6C^+Ly6G^+$ PMN-MDSC precursors were significantly decreased in *ΔNp63* icKO tumor-bearing mice, suggesting that *ΔNp63* icKO tumors have a decreased number of circulating double-positive MDSCs, which may relate to less infiltration of MDSCs in primary tumors and metastasis in lymph nodes (Figure S1L). Our results show that conditional loss of ΔNp63 in established tumors is responsible for reduced survival of MDSCs and is associated with decreased tumor progression and metastasis of spontaneously developed tumors.

Genetic loss of ΔNp63 inhibits tumor progression and metastasis in a metastatic syngeneic TNBC mouse model

Because MMTV-Wnt1 mice have rare lung metastasis when tumors are palpable,[25] we wanted to test the highly metastatic syngeneic 4T1 TNBC mouse model to evaluate the effect of ΔNp63 on MDSCs associated with metastasis. To further understand the function of ΔNp63 in progression of developed aggressive cancers, we employed CRISPR knockout (KO) in developed 4T1 TNBC tumors. We used doxycycline-inducible lentiviral expression of Cas9[32] to induce genetic loss of *ΔNp63* after tumors were developed (Figure 2A). Mouse 4T1 TNBC cells were used, which are aggressive and metastatic. Further, tumors from 4T1 cells resemble TNBC tumors in patients in the clinic.[33] 4T1 cells were transduced with inducible Cas9 lentivirus followed by individual single guide RNAs (sgRNAs) targeting *ΔNp63*. Two independent sgRNAs for inducible KO (iKO) of *ΔNp63* (iKO1 and iKO2) were used. Successful *ΔNp63* iKO was confirmed with western blotting of *ΔNp63* iKO cells vs. control (Figure 2B). KO of *ΔNp63* by doxycycline in food using iKO1 and iKO2 showed that loss of ΔNp63 leads to reduced

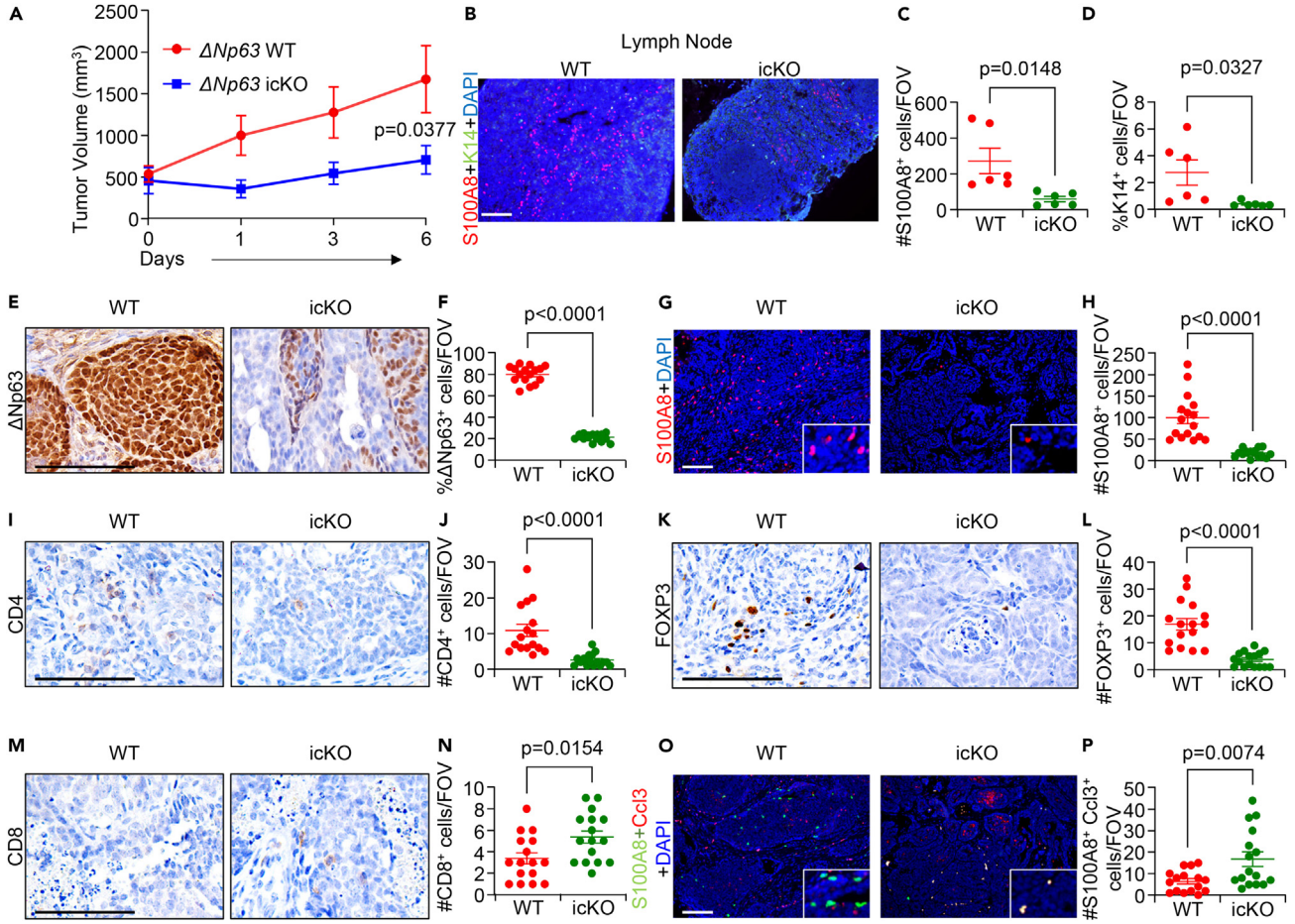

Figure 1. Inducible conditional knockout of *ΔNp63* in tumor cells decreased tumor growth and MDSC number in TNBC GEMM

(A) *MMTV-Wnt1;iK14-Cre*$^{+}$*;ΔNp63*$^{f/f}$ mice (icKO) with developed mammary tumor were injected with tamoxifen (70 μg/mouse/day for 3 days) to induce conditional KO (icKO) of *ΔNp63*. icKO of *ΔNp63* reduced growth of developed TNBC compared to *ΔNp63* WT (*MMTV-Wnt1;iK14-Cre*$^{-}$*;ΔNp63*$^{f/f}$ or *MMTV-Wnt1;iK14-Cre*$^{+}$*;ΔNp63*$^{f/f}$) mice. For WT, vehicle control corn oil was administered to mice. n = 7 tumors/group.

(B–D) Mice were sacrificed on day 6, and axillary lymph nodes were stained with S100A8 (red) and K14 (green) antibodies. *ΔNp63* icKO lymph nodes showed decreased S100A8^{+} MDSCs and K14^{+} tumor cells compared to *ΔNp63* WT mice. n = 6 lymph nodes/group.

(E and F) IHC was performed in tumor tissues from *ΔNp63* WT and *ΔNp63* icKO mice. icKO of *ΔNp63* by tamoxifen-inducible Cre was demonstrated with decreased ΔNp63 staining in *ΔNp63* icKO mice compared to *ΔNp63* WT mice. n = 3 tumors/group.

(G and H) S100A8^{+} cells (red) were decreased in *ΔNp63* icKO mice compared to *ΔNp63* WT mice. n = 3 tumors/group.

(I–N) *ΔNp63* icKO mice showed decreased CD4^{+} T-cells and FOXP3^{+} T-cells compared to *ΔNp63* WT mice. CD8^{+} T-cells were increased in *ΔNp63* icKO mice compared to *ΔNp63* WT mice. n = 3 tumors/group.

(O and P) Co-immunostaining with S100A8 and cleaved caspase 3 (Ccl3) antibodies revealed that *ΔNp63* icKO tumors have higher S100A8^{+}Ccl3^{+} cells (yellow color) compared to *ΔNp63* WT tumors. n = 3 tumors/group. For all IHC/IF images, 16 random fields of view (FOVs) were chosen from 3 tumors/group. p values were calculated using two-way ANOVA with Bonferroni post-test adjustment (A) and two-tailed unpaired Student's *t* test (C, D, F, H, J, L, N, P). (A, C, D, F, H, J, L, N, P) Data are presented as the mean ± SEM. Scale bars, 100 μm (B, E, G, I, K, M, O).

tumor growth (Figures 2C–2F). To determine the effect of loss of ΔNp63 on metastasis in TNBC, lungs were examined, and metastatic nodules were counted. KO of *ΔNp63* by both iKO1 and iKO2 in 4T1 tumor-bearing mice showed decreased lung metastatic nodules, suggesting that loss of ΔNp63 in advanced tumors is associated with reduced lung metastasis (Figures 2G–2J). It is possible that reduced metastasis may be due to fewer circulating tumor cells from the reduced primary tumors with *ΔNp63* KO rather than altered metastatic characteristics of the cancer cells. Therefore, we intravenously injected equal numbers of control 4T1 cells or *ΔNp63* iKO1 4T1 cells followed by doxycycline treatment. *ΔNp63* iKO1 4T1 cells showed less colonization in lungs, consistent with the orthotropic model, proving evidence that ΔNp63 is essential to promote metastasis (Figures 2K and 2L). When 4T1 cells carrying the empty vector were administered to mice as control, there was no reduction in tumor growth and ΔNp63 protein by doxycycline treatment, suggesting that the changes found were not caused by doxycycline treatment but by *ΔNp63* iKO. (Figures S2A and S2B). Thus, our results revealed that genetic loss of *ΔNp63* inhibited tumor progression and metastasis in developed TNBC *in vivo*.

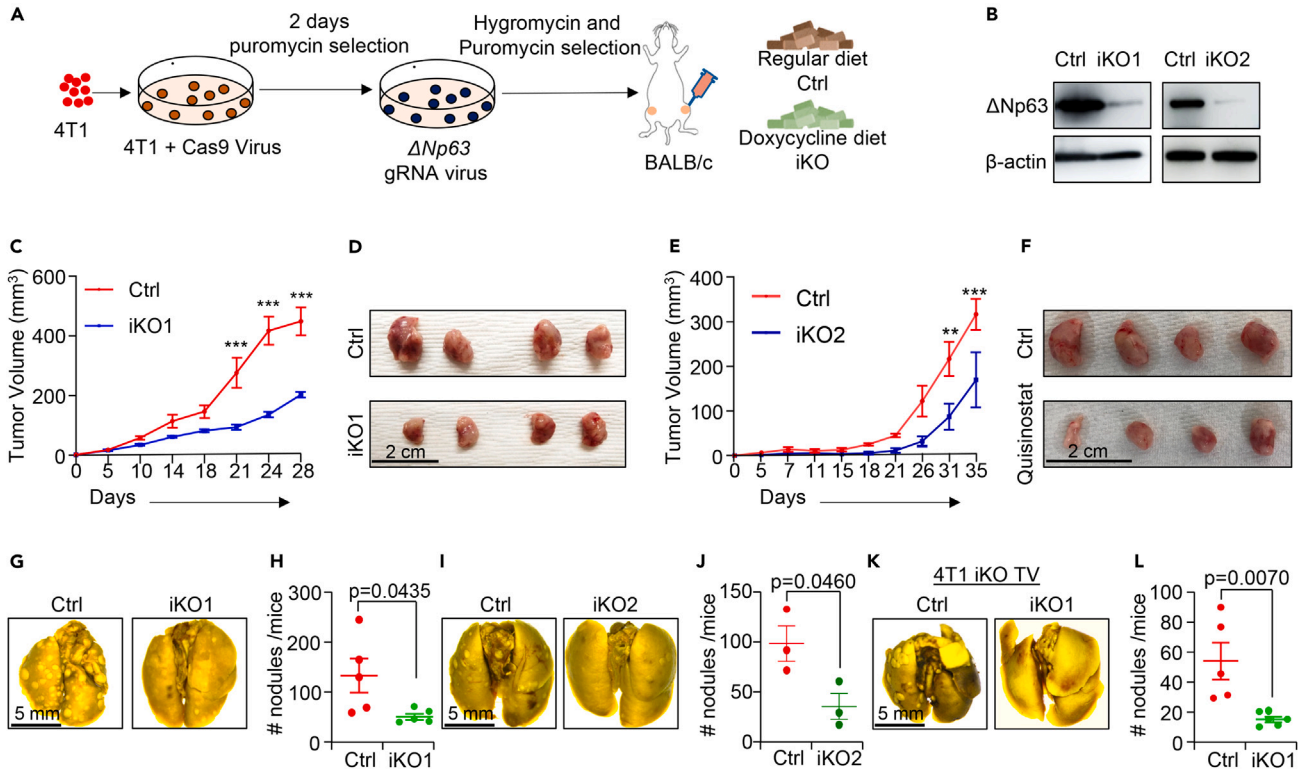

Figure 2. Inducible conditional KO of *ΔNp63* by CRISPR/Cas9 system decreased tumor progression and lung metastasis in 4T1 TNBC syngeneic mouse model

(A) Mouse 4T1 TNBC cells were infected with pCW-Cas9 virus followed by *ΔNp63* sgRNA virus and screened with 0.5 μg/mL puromycin and 20 μg/mL hygromycin. The established *ΔNp63* iKO 4T1 cells were injected into mammary fat pads of BALB/c mice. When tumors grew 3 × 3 mm, doxycycline food was fed for *ΔNp63* iKO.

(B) Genetic loss of *ΔNp63* in *ΔNp63* iKO 4T1 cells was confirmed with western blotting. 2 μg/mL doxycycline was given for 48 h.

(C) The tumors in BALB/c mice with control 4T1 or *ΔNp63* iKO1 4T1 cells were palpated, and tumor growth curve was plotted. n = 6 tumors/group.

(D) The tumors were harvested, and representative images showed that *ΔNp63* iKO1 decreased tumor growth compared to control (-DOX).

(E) BALB/c mice were injected with control 4T1 or *ΔNp63* iKO2 4T1 cells, and tumor growth curve was plotted. n = 4 tumors/group.

(F) The tumors were harvested, and representative images were taken. Similar to *ΔNp63* iKO1, tumor growth was inhibited in *ΔNp63* iKO2 tumors compared to control (-DOX).

(G and H) Lung was fixed with Bouin's solution to count metastatic nodules. *ΔNp63* iKO1 tumor-bearing mice showed less metastatic nodules compared to control (-DOX). n = 5 mice/group.

(I and J) Similar to *ΔNp63* iKO1 mice, lungs from *ΔNp63* iKO2 mice were fixed with Bouin's solution and metastatic nodules were examined. *ΔNp63* iKO2 tumor-bearing mice showed decreased number of metastatic nodules compared to control (-DOX). n = 3 mice/group.

(K) Control 4T1 or *ΔNp63* iKO1 4T1 cells were intravenously injected in BALB/c mice, and lung was examined for metastasis.

(L) *ΔNp63* iKO1 4T1 cells showed impaired colonization in the lung compared to control (-DOX). n = 5 control, n = 6 iKO1. p values were calculated using two-way ANOVA with Bonferroni post-test adjustment (C, E) and two-tailed unpaired Student's *t* test (H, J, L). $^{**}p < 0.01$, $^{***}p < 0.001$. (C, E, H, J, L) Data are presented as the mean ± SEM. Scale bars, 2 cm (D, F), 5 mm (G, I, K).

Genetic loss of ΔNp63 affects the tumor-favorable immune microenvironment by reducing MDSCs

To evaluate ΔNp63 levels, IHC was performed with *ΔNp63* iKO1 and iKO2 4T1 tumors. The ΔNp63 IHC results confirmed that the ΔNp63 loss in 4T1 cells was maintained in tumors *in vivo* (Figures 3A, 3B, S2C, and S2D). Since we observed a delayed tumor progression of *ΔNp63* iKO tumors, we evaluated proliferation and cell death of tumor cells. We found that the number of $Ki67^+$ (proliferating) cells decreased in *ΔNp63* iKO tumors (Figures 3C, 3D, S2E, and S2F), whereas the apoptotic marker $Ccl3^+$ cells increased (Figures 3E, 3F, S2G, and S2H), suggesting that ΔNp63 simultaneously affects cell proliferation and cell death. IF staining with S100A8 antibody showed a decrease in MDSC numbers in *ΔNp63* iKO tumors, indicating that targeting ΔNp63 can reduce MDSCs even in established tumors (Figures 3G, 3H, S2I, and S2J). IHC of *ΔNp63* iKO tumors revealed a decrease in $CD4^+$ T-cells (Figures 3I, 3J, S2K, and S2L) and $FOXP3^+$ regulatory T-cells (Figures 3K, 3L, S2M, and S2N), and an increase in cytotoxic $CD8^+$ T-cells (Figures 3M, 3N, S2O, and S2P). This implies that ΔNp63 loss decreases T cell suppression due to reductions in the MDSC population. Consistent with IF and IHC results, flow cytometry of *ΔNp63* iKO tumors showed a trend of decreased MDSCs ($p = 0.08$) (Figure 3O), increased $CD4^-CD8^+$ T-cells (Figure 3P), and decreased $CD4^+CD8^-$ T-cells (Figure 3Q). Thus,

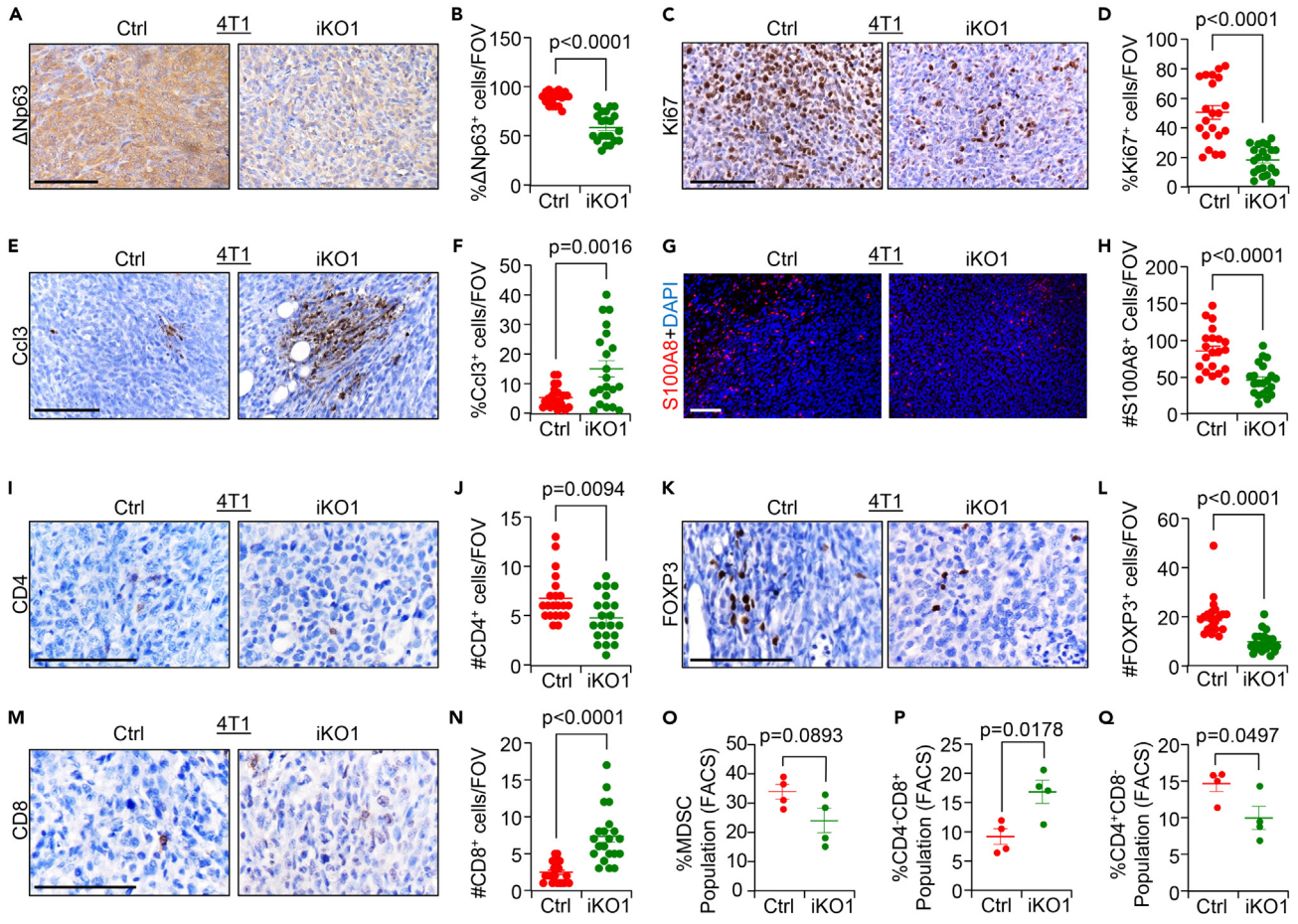

Figure 3. Histopathological and flow cytometric analysis revealed that genetic loss of *ΔNp63* by CRISPR method decreased tumor growth by reshaping immune cell populations in TNBC

(A–F) IHC was performed with tumors from mice with mammary fat pads injection of control 4T1 and *ΔNp63* iKO1 4T1 cells. IHC showed decreased ΔNp63 levels in the *ΔNp63* iKO1 4T1 tumors compared to control (-DOX). *ΔNp63* iKO1 also decreased proliferative marker Ki67 in tumors, while increasing apoptotic marker cleaved caspase 3 (Ccl3) compared to control (-DOX). n = 4 tumors/group.

(G and H) IF was performed with MDSC marker S100A8 (red) antibody in the ΔNp63 *iKO1* and control 4T1 tumors. *ΔNp63* iKO1 tumor showed decreased number of tumor-infiltrating MDSCs compared to control (-DOX). n = 4 tumors/group.

(I–N) *ΔNp63* iKO1 4T1 tumors showed decreased $CD4^+$ helper T-cells and $FOXP3^+$ regulatory T-cells, while increasing $CD8^+$ cytotoxic T-cells compared to control (-DOX). n = 4 tumors/group (O–Q) Flow cytometric analysis revealed altered immune populations. Consistent with histopathological results, *ΔNp63* iKO1 tumors showed lower MDSC number compared to control (-DOX) (p = 0.0893). $CD4^-CD8^+$ cytotoxic T-cells were increased while $CD4^+CD8^-$ helper T-cells were decreased in *ΔNp63* iKO1 tumors compared to control (-DOX). n = 4 tumors/group. For all IHC/IF images, 21 random fields of view (FOVs) were chosen from 4 tumors/group. p values were calculated using two-tailed unpaired Student's *t* test (B, D, F, H, J, L, N, O, P, Q). Data are presented as the mean ± SEM. Scale bars, 100 μm (A, C, E, G, I, K, M).

our histological results with allografts corroborate our GEMM model and demonstrate a strong connection between ΔNp63 and MDSCs in TNBC tumors.

Pharmacological inhibition of ΔNp63 suppresses tumor progression and metastasis in TNBC

Napoli et al. reported that HDAC inhibitor (HDACi) Quisinostat significantly reduced the expression of ΔNp63 in MCF-10A cells.[34] Quisinostat is well known for its prolonged pharmacodynamic effects *in vivo* and antitumor efficacy compared to other analogs.[35] Therefore, we tested the effect of Quisinostat on ΔNp63 in advanced and metastatic TNBC tumors. We injected 4T1 cells into mammary fat pads of BALB/c mice. When tumors reached ~65 mm^3, mice were treated with vehicle or Quisinostat (Figure 4A). Quisinostat significantly inhibited the progression of TNBC, suggesting that it has an inhibitory effect on development of TNBC primary tumors (Figures 4B and 4C). Reduced ΔNp63 protein levels were confirmed in Quisinostat-treated 4T1 cells by western blot (Figure 4D). It has been reported that HDACi regulates the levels of ΔNp63 protein via FBXW7 in cutaneous squamous cell carcinoma.[34] E3 ligases MDM2 and FBXW7 cooperate with each other for degradation of ΔNp63 protein.[36] Our western blot results show that Quisinostat increases FBXW7 protein levels in a dose-dependent manner, suggesting

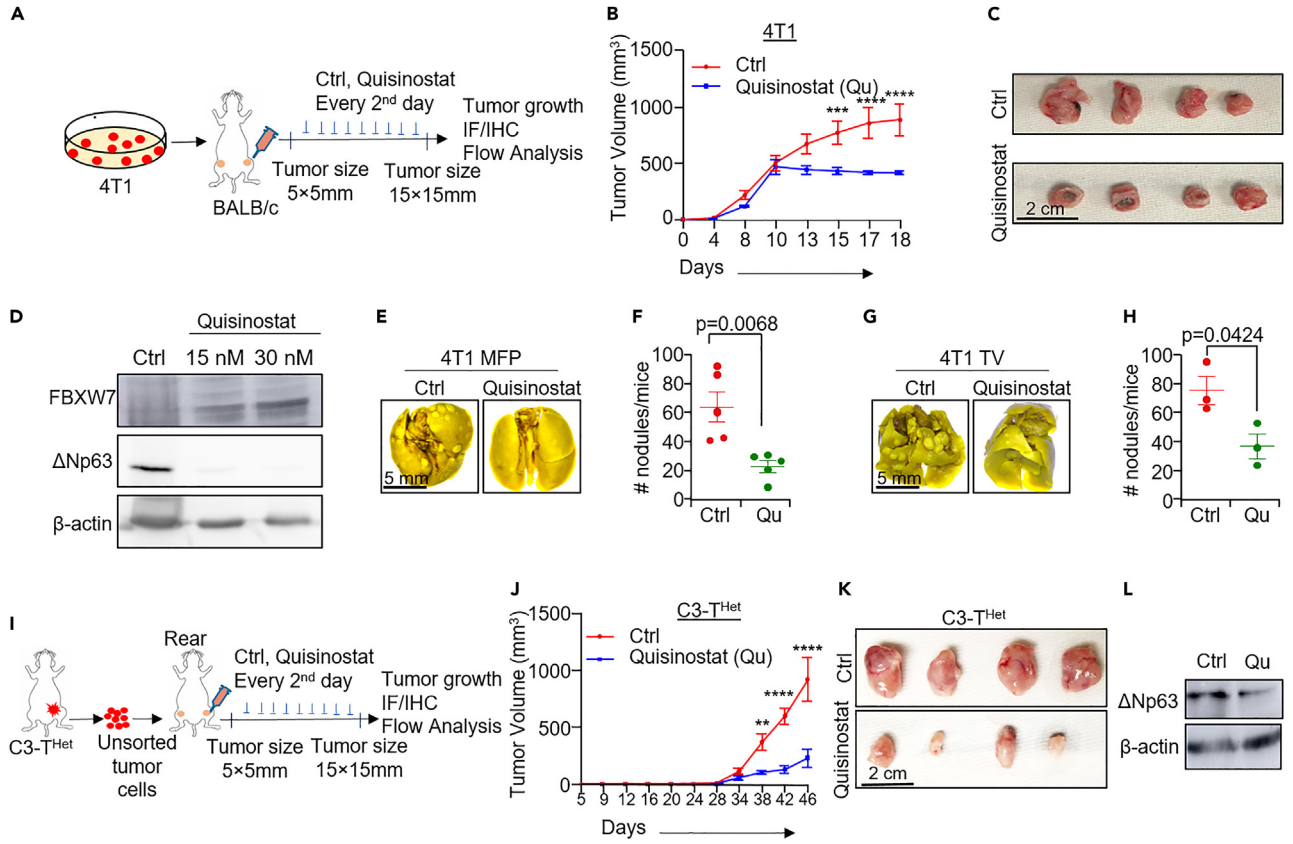

Figure 4. Pharmacological loss of ΔNp63 with Quisinostat decreased tumor growth and lung metastasis in TNBC syngeneic mouse models

(A) 4T1 cells were injected into mammary fat pads of BALB/c mice. Mice were treated with vehicle or 40 mg/kg HDACi Quisinostat (Qu) every other day by intraperitoneal injection.

(B) Quisinostat dramatically inhibited tumor growth of 4T1 cells compared to vehicle. n = 6 control, n = 8 Quisinostat.

(C) Representative images of tumors.

(D) 4T1 cells were treated *in vitro* with Quisinostat, which decreased the protein level of ΔNp63 compared to control. FBXW7 levels were increased with increased dose of Quisinostat.

(E) Lung metastasis was analyzed in mammary fat pads injected 4T1 mice.

(F) Quisinostat decreased metastatic nodules of lung compared to vehicle. n = 5 mice/group.

(G) 4T1 cells were intravenously injected in BALB/c mice and followed by vehicle or Quisinostat injection. Lungs were fixed with Bouin's solution to check metastasis.

(H) Quisinostat reduced metastatic lung nodules in tail-vein-injected 4T1 mice compared to vehicle. n = 3 mice/group.

(I) Primary tumors from C3(1)/Tag (C3-T); $Elf5^{+/-}$ (^{Het}) mice were isolated into single cells and injected into mammary fat pads of Rear mice. Mice were injected with vehicle or 40 mg/kg Quisinostat every other day.

(J) Quisinostat decreased growth of C3-T^{Het} tumor compared to vehicle. n = 6 tumors/group.

(K) Representative image of tumors.

(L) C3-T^{Het} tumors were subjected to western blot. ΔNp63 protein levels were decreased in C3-T^{Het} tumors treated with Quisinostat compared to vehicle. p values were calculated using two-way ANOVA with Bonferroni post-test adjustment (B, J) and two-tailed unpaired Student's *t* test (F, H). $^{**}p < 0.01$, $^{***}p < 0.001$, $^{****}p < 0.0001$. (B, F, H, J) Data are presented as the mean ± SEM. Scale bars, 2 cm (C, K). 5 mm (E, G).

that Quisinostat controls FBXW7-dependent regulation of ΔNp63 protein levels by increasing FBXW7 protein levels in TNBC (Figure 4D). To evaluate the effect of Quisinostat-mediated ΔNp63 loss on TNBC metastasis, lungs were examined. We found that Quisinostat significantly reduced lung metastatic nodules (Figures 4E and 4F). To evaluate metastasis with the same number of cancer cells, 4T1 cells were injected into the tail vein of mice and treated with Quisinostat. Similar to the results of the orthotopic model, Quisinostat inhibited lung metastasis in experimental assay, suggesting that it can inhibit TNBC metastasis (Figures 4G and 4H).

To further understand the effect of ΔNp63 inhibition by Quisinostat in an independent TNBC model, we orthotopically implanted primary tumor cells from mammary tumors of C3(1)/Tag (C3-T); $Elf5^{+/-}$ (^{Het}) mice into C3-T-Rear (Rear) mice, which bear all functional immune cells including T-cells and MDSCs but are also tolerant to tumors carrying C3-T antigen.[37] Importantly, in a previous report we demonstrated that C3-T^{Het} spontaneous tumors represent an aggressive TNBC model with high incidence of lung metastasis (Figure 4I).[38] Here again,

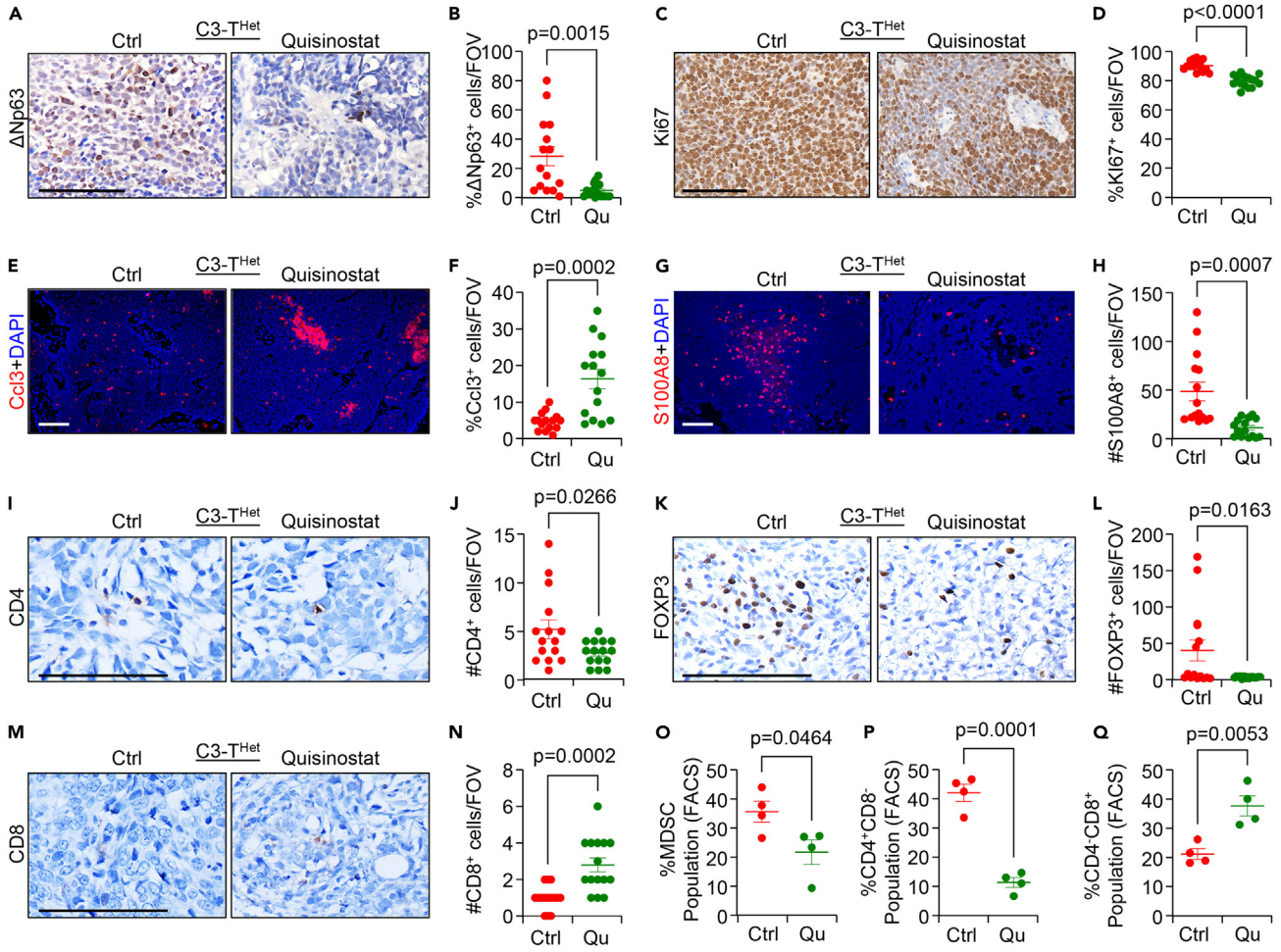

Figure 5. Pharmacological loss of ΔNp63 with Quisinostat decreased tumor growth in C3-T^{Het} tumor by changing the immune landscape in TNBC

(A–D) Tumors from C3-T^{Het} mice were isolated into single cells and injected into mammary fat pads of Rear mice. IHC was performed with vehicle or HDACi Quisinostat-treated C3-T^{Het} tumors. IHC confirmed decreased ΔNp63 levels in the Quisinostat-treated C3-T^{Het} tumors compared to vehicle. Quisinostat also decreased proliferative marker Ki67 compared to vehicle. n = 3 tumors/group.

(E–H) IF was performed with vehicle or HDACi Quisinostat-treated C3-T^{Het} tumors. The apoptotic marker cleaved caspase 3 (Ccl3) was stained (red). Quisinostat-treated tumors showed an increased number of Ccl3$^+$ cells in tumor compared to vehicle. IF was also performed with MDSC marker S100A8 (red color) antibody in the Quisinostat-treated tumors. Quisinostat-treated tumors showed a decreased number of tumor-infiltrating MDSCs compared to vehicle. n = 3 tumors/group.

(I–N) Quisinostat-treated tumors showed decreased CD4$^+$ helper T-cells and FOXP3$^+$ regulatory T-cells, while increasing CD8$^+$ cytotoxic T-cells compared to vehicle. n = 3 tumors/group.

(O–Q) Flow cytometric analysis of tumors with Quisinostat treatment showed decreased number of MDSCs and CD4$^+$CD8$^-$ helper T-cells and increased number of CD4$^-$CD8$^+$ cytotoxic T-cells compared to vehicle. n = 4 tumors/group. For all IHC/IF images, 15 random fields of view (FOVs) were chosen from 3 tumors/group. p values were calculated using two-tailed unpaired Student's *t* test (B, D, F, H, J, L, N, O, P, Q). Data are presented as the mean ± SEM. Scale bars, 100 μm (A, C, E, G, I, K, M).

Quisinostat was effective in reducing primary C3-T^{Het} tumor burden, showing its therapeutic efficacy against multiple aggressive TNBC models (Figures 4J and 4K). Western blot with primary tumor proved that Quisinostat treatment decreased ΔNp63 protein levels *in vivo* (Figure 4L). Taken together, our results show that the HDACi Quisinostat inhibits TNBC tumor progression and metastasis by inhibiting ΔNp63.

Quisinostat-mediated pharmacological loss of ΔNp63 decreases MDSC-mediated tumor progression

Since pharmacological loss of ΔNp63 by Quisinostat phenocopied the inhibition of tumor growth and metastasis induced by genetic loss, we evaluated histological changes in tumor by Quisinostat. After administering Quisinostat to C3-T^{Het} mice, which are an aggressive TNBC model, immunostaining was performed on the C3-T^{Het} tumors. Quisinostat was found to effectively reduce the level of ΔNp63 *in vivo* suggesting that the resulting phenotypic changes were attributed to reduced ΔNp63 (Figures 5A and 5B). A decrease in Ki67 by IHC and an increase in Ccl3 by IF also showed that tumor progression was inhibited by reducing cancer cell proliferation and increasing apoptosis

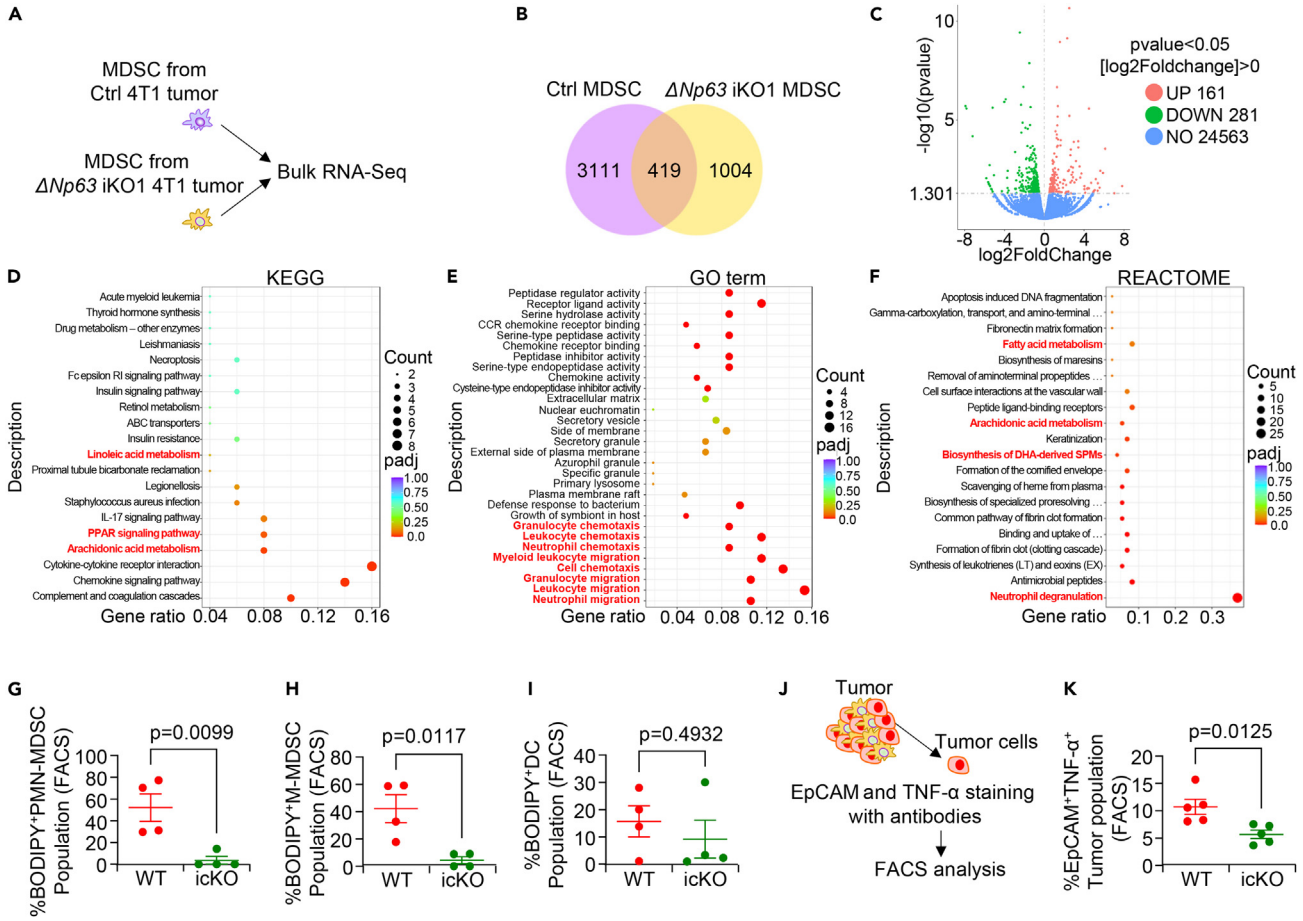

Figure 6. MDSCs from *ΔNp63* iKO1 tumors showed altered signature of chemotaxis and metabolism

(A) MDSCs were isolated from *ΔNp63* control and *ΔNp63* iKO1 4T1 TNBC tumors followed by bulk RNA-seq. n = 2 tumors/group.

(B) Venn Diagram showed differentially expressed 4,115 genes (3,111 up genes in control MDSCs, 1,004 up genes in *ΔNp63* iKO1 MDSCs).

(C) Volcano plot revealed 161 upregulated genes and 281 downregulated genes in *ΔNp63* iKO1 MDSCs compared to *ΔNp63* WT MDSCs.

(D) KEGG enriched pathway showed association of lipid metabolism in *ΔNp63* iKO1 MDSCs.

(E) Altered pathways such as chemotaxis and migration were also identified with GO term.

(F) REACTOME enrichment analysis revealed that *ΔNp63* iKO1 is involved in lipid metabolism and degranulation of neutrophils.

(G–I) *MMTV-Wnt1;iK14-Cre*$^{+}$*;ΔNp63*$^{f/f}$ mice (icKO) with developed mammary tumor injected with tamoxifen in corn oil (as described in Figure 1) to induce conditional KO (icKO) of *ΔNp63*. *ΔNp63* WT mice (*MMTV-Wnt1;iK14-Cre*$^{-}$*;ΔNp63*$^{f/f}$ or *MMTV-Wnt1;iK14-Cre*$^{+}$*;ΔNp63*$^{f/f}$) were injected with vehicle corn oil only. Tumor tissues were digested into single cells and incubated with antibodies for flow and BODIPY for neutral lipid staining. Flow analysis revealed that *ΔNp63* icKO tumors have lower BODIPY^{+} PMN-MDSCs, M-MDSCs, but not DCs. n = 4 tumors/group.

(J and K) EpCAM^{+}TNF-α^{+} tumor populations were analyzed by flow analysis, which revealed that *ΔNp63* icKO tumors have decreased EpCAM^{+}TNF-α^{+} cells. n = 5 tumors/group. p values were calculated using two-tailed unpaired Student's *t* test (G, H, I, K). Data are presented as the mean ± SEM.

(Figures 5C–5F). In support, we found that, similar to the *ΔNp63* genetic deletion model, Quisinostat reduced the number of MDSCs (Figures 5G and 5H), CD4^{+} T-cells (Figures 5I and 5J), and FOXP3^{+} T-cells, suggesting that tumor progression was inhibited by a decrease in immunosuppressive T-cells (Figures 5K and 5L). Quisinostat also increased CD8^{+} T-cells generating an increased ratio of cytotoxic T-cells to tumor supporting T-cells (Figures 5M and 5N). The changes of immune cells observed histologically were also confirmed by flow cytometry (Figures 5O–5Q). Results from Quisinostat-treated C3-T^{Het} tumors were further corroborated with Quisinostat-treated 4T1 tumors (Figures S3A–S3I). Our results show that Quisinostat inhibits TNBC growth by changing the composition of immune cells, similar to genetic deletion of *ΔNp63*.

MDSCs from ΔNp63 iKO TNBC tumor show altered signatures in lipid metabolism and chemotaxis

To further understand how *ΔNp63* iKO affects MDSCs in TNBC, we performed bulk RNA sequencing (RNA-seq) with isolated MDSCs from control or *ΔNp63* iKO1 4T1 TNBC tumors and identified differentially expressed genes (Figures 6A–6C). Kyoto Encyclopedia of Genes and Genomes (KEGG) analysis showed that the differentially expressed mRNAs were related to pathways in lipid metabolism such as linoleic acid

metabolism, peroxisome proliferator-activated receptor (PPAR) signaling pathway, and arachidonic acid (Figure 6D). Linoleic acid,[39] arachidonic acid,[40] and fatty acid oxidation by PPARγ[41] can boost immunosuppressive activity of MDSCs, implying that compromised lipid metabolism of MDSCs might contribute to the decreased immune suppression in *ΔNp63* iKO1 tumors. We also found that MDSCs from *ΔNp63* iKO1 tumors downregulated several signatures relating to chemotaxis and migration of MDSCs (Figure 6E), suggesting ΔNp63 may recruit MDSCs via alterations in the tumor cell secretome. Consistent with the KEGG analysis, REACTOME-enriched pathways also indicated that MDSCs from *ΔNp63* iKO1 were involved in several lipid metabolism pathways such as fatty acid metabolism, arachidonic acid metabolism, and biosynthesis of docosahexaenoic acid (DHA)-derived specialized pro-resolving mediators (SPMs) (Figure 6F). The enriched REACTOME pathways also revealed neutrophil degranulation of MDSCs (Figure 6F), which is required for their immunosuppressive activity.[42] The reduced chemotaxis and recruitment gene signature in MDSCs from *ΔNp63* iKO1 tumor were supported by IF analysis showing decreased MDSC number in tumors (Figures 1G, 1H, 3G, 3H, 5G, and 5H). To experimentally validate the changes in the lipid signature, neutral lipids in *ΔNp63* WT MMTV-Wnt1 and *ΔNp63* icKO MMTV-Wnt1 tumors were stained with BODIPY and BODIPY$^+$ populations were analyzed. BODIPY$^+$ PMN-MDSCs and M-MDSCs in *ΔNp63* icKO MMTV-Wnt1 tumor were significantly decreased compared to *ΔNp63* WT MMTV-Wnt1 tumor (Figures 6G and 6H). Notably, interrogation of additional immune populations in tumors such as DCs showed no significant change (Figure 6I), implying MDSC-specific lipid reprogramming by *ΔNp63* in tumor.

We next examined the mechanism of *ΔNp63* on MDSC survival. *In silico* analysis of existing RNA-seq data[16] shows that loss of ΔNp63 decreases TNF-α pathway genes (TNF-α, JunB, etc) (data not shown). It is reported that TNF-α signaling can paradoxically promote MDSC survival in certain tumors through TNFR2.[43] Therefore, we analyzed TNF-α$^+$ in EpCAM$^+$ tumor cell populations (Figure 6J). *ΔNp63* icKO tumor showed decreased TNF-α$^+$ in tumor cells (Figure 6K), suggesting that secreted TNF-α from ΔNp63$^+$ tumor cells may aid in survival of MDSC in the tumor microenvironment of TNBC. Overall, these results indicate ΔNp63 can alter gene signatures in metabolism and chemotaxis of MDSCs, affecting immunosuppressive activity and recruitment of MDSCs. ΔNp63$^+$ tumor cells can regulate lipid metabolism, and MDSC survival is promoted in a TNF-α-dependent manner.

Overexpression of ΔNp63 promotes tumor progression and metastasis with increased infiltration of MDSCs in TNBC

To deepen our understanding of ΔNp63, we overexpressed WT *ΔNp63* and R304W *ΔNp63* with mutation in the DNA-binding domain (*ΔNp63*-mt) in 4T1 cells. qPCR and western blot (WB) demonstrated overexpressed mRNA and protein levels (Figures 7A and 7B). To determine the effect of *ΔNp63* overexpression (OE) on tumor progression and metastasis, 4T1 cells were injected into the mammary fat pads of BALB/c mice and tumor growth was measured. The tumor growth of *ΔNp63* OE tumors was significantly accelerated compared to control empty vector (Ctrl) and *ΔNp63*-mt OE (Figures 7C and 7D). Lung metastatic nodules showed increased metastasis in *ΔNp63* OE mice compared to Ctrl and *ΔNp63*-mt OE mice (Figures S4A and S4B). FACS analysis was performed to evaluate whether progression by *ΔNp63* OE was accompanied by changes in the immune microenvironment. MDSCs but not TAMs and DCs show significant increase in number in *ΔNp63* OE tumors compared to Ctrl and *ΔNp63*-mt OE tumors, suggesting *ΔNp63* OE was associated with changes in MDSC populations (Figures 7E, S4C, and S4D). To understand role of *ΔNp63* OE in lipid metabolism of MDSCs, neutral lipid of MDSCs in *ΔNp63* OE and *ΔNp63*-mt OE 4T1 tumors was analyzed by staining them with BODIPY (Figure 7F). MDSCs from *ΔNp63* OE tumors show an increased BODIPY$^+$ population compared to control and *ΔNp63*-mt OE, suggesting that ΔNp63$^+$ tumor plays an important role in lipid metabolism of MDSCs (Figure 7G). Furthermore, tumor cells showed increased trend to TNF-α$^+$ population in *ΔNp63* OE tumors compared to control and *ΔNp63*-mt OE tumors (Figure 7H), supporting loss of function data. We also evaluated the expression levels of *Tnfr1* and *Tnfr2*, which are TNF-α receptors, in MDSCs (Figures 7I and S4E). We found no significant difference in receptor levels in MDSC, suggesting that increased TNF-α in tumor cells may have influenced the MDSC survival. Our experiments with *ΔNp63* OE models support the results of *ΔNp63* icKO and iKO mouse experiments and show that ΔNp63-induced tumor progression and metastasis are associated with MDSCs.

Combinatorial targeting of ΔNp63 along with chemotherapy sensitizes TNBC to chemotherapy

Conventional chemotherapy is the standard therapy chosen for TNBC, but chemoresistance leads to early recurrence and metastasis, which negatively affects the patient's prognosis.[44] Therefore, development of better drug combinations with targeted therapy to sensitize TNBC to chemotherapy is needed. Based on the results showing that targeting ΔNp63 inhibits TNBC tumor progression and metastasis, we evaluated whether ΔNp63 targeting can sensitize TNBC to conventional chemotherapy. Doxorubicin was administered to mice bearing 4T1 tumors as chemotherapy, with doxycycline used to induce KO of *ΔNp63* (Figures 8A, 8B, and S5A). Chemotherapy alone partially inhibited TNBC, and combination with ΔNp63 inhibition by doxycycline inhibited tumor growth more than chemotherapy alone, indicating that genetic loss of *ΔNp63* sensitizes TNBC to chemotherapy. Similar to genetic loss of *ΔNp63*, co-administration of Quisinostat and chemotherapy showed increased tumor suppression than chemotherapy alone (Figures 8C and 8D). Combination therapy with iKO of *ΔNp63* or Quisinostat also decreased lung metastasis, suggesting targeting ΔNp63 in combination with chemotherapy in established advanced tumors also significantly inhibited metastasis (Figures 8E, 8F, and S5B). Furthermore, we also found that combination treatment reduced MDSC number significantly in tumors (Figures 8G, 8H, S5C, and S5D). Ccl3$^+$ MDSCs were analyzed to investigate whether the decreased MDSC number was related to the survival of MDSCs. We found that the combination of chemotherapy and Quisinostat decreased survival of MDSCs by significantly increasing apoptosis (Figures 8I and 8J). These results show that conventional chemotherapy is indeed insufficient for ΔNp63$^+$ tumors, and that inhibition of ΔNp63 sensitizes tumors to chemotherapy treatment, opening potential new avenues for treatment to advanced TNBC patients.

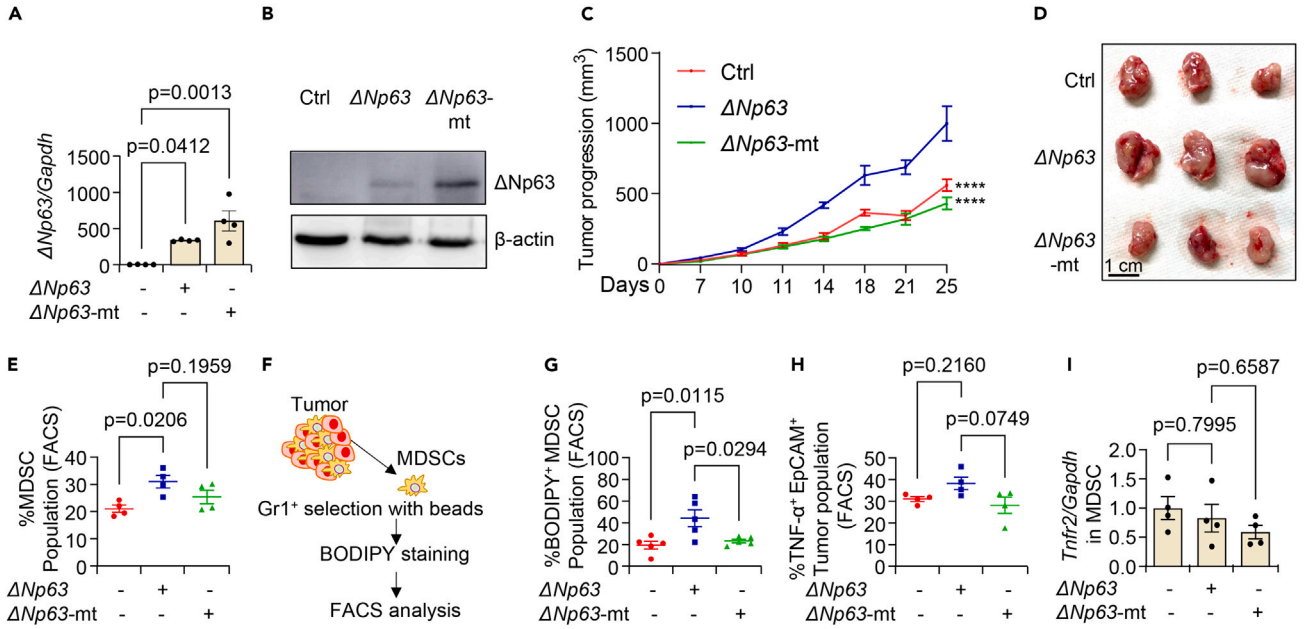

Figure 7. Overexpression of *ΔNp63* augmented tumor progression and metastasis of TNBC with increased MDSCs

(A and B) 4T1 cells with overexpression (OE) of *ΔNp63* and mutant *ΔNp63* (*ΔNp63*-mt) were confirmed by qPCR and western blot. n = 4/group.

(C and D) The cells were injected into mammary fat pads of BALB/c mice. *ΔNp63* OE dramatically facilitated tumor growth of 4T1 cells compared to control (empty vector) and *ΔNp63*-mt OE. n = 5 tumors/group.

(E) FACS analysis revealed that *ΔNp63* OE increased MDSCs compared to control and *ΔNp63*-mt OE 4T1 tumor. n = 4 tumors/group.

(F and G) 4T1 tumors with overexpression (OE) of *ΔNp63* and *ΔNp63*-mt were digested and enriched with magnetic beads attached to Gr1 antibody. Enriched MDSCs were subjected to BODIPY staining and flow analysis. *ΔNp63* OE tumors have a higher number of BODIPY$^+$ MDSC populations compared to control and *ΔNp63*-mt OE tumors. n = 5 tumors/group.

(H) Tumor cells were enriched with EpCAM antibody from 4T1 tumors. Enriched tumor cells were subjected to FACS with TNF-α antibody. *ΔNp63* OE tumors showed increased TNF-α compared to MCS and *ΔNp63*-mt OE 4T1 tumors n = 4 tumors/group.

(I) RNA was extracted from enriched MDSCs and subjected to qPCR. The expression of *Tnfr2* showed no significant differences n = 4 tumors/group. p values were calculated using one-way ANOVA with Tukey's multiple-comparisons *post hoc* test (A, E, G, H, I) and two-way ANOVA with Bonferroni post-test adjustment (C). ****p < 0.0001. (A, C, E, G, H, I) Data are presented as the mean ± SEM. Scale bars, 1 cm (D).

DISCUSSION

Because TNBC is negative for targetable hormonal receptors, it does not respond to hormone therapy or HER2-targeted therapy, forcing conventional chemotherapy as the main treatment option. However, less than 30% of TNBC patients show a complete response,[5] and more than 50% relapse 3 to 5 years after initial diagnosis.[6] The need for suitable animal models and targets for studying chemoresistance of TNBC clearly shows a gap in the field. To fill the gap, we used GEMM and syngeneic models of TNBC, where targeting ΔNp63 sensitized tumors to chemotherapy. We previously found that ΔNp63 is a key regulator of mammary gland homeostasis[30] and a major driver of TNBC proliferation and metastasis.[16] Mouse models with injected TNBC tumor cells harboring *ΔNp63* knockdown had delayed TNBC initiation and reduced tumor burden, and this result was recapitulated in *ΔNp63* icKO mice, suggesting that *ΔNp63* plays an important role in TNBC development.[17] However, TNBC patients undergoing chemotherapy receive treatment after the tumor is diagnosed. Therefore, in this study, we decided to evaluate the effect of inhibiting ΔNp63 in established TNBC with inducible GEMM and syngeneic models. Conditional knockout of *ΔNp63* in advanced tumors suppressed TNBC progression and metastasis in multiple models with differing methodologies, implying that ΔNp63 has potential as a target for a broad spectrum of TNBC clinical cases.

Among the hallmarks of cancer, the role of immune cells is increasingly emphasized.[45] However, the effect of ΔNp63 on the immune population of TNBC is not well known. In the previous experiments, we reported higher number of MDSCs and expression of *ΔNp63* in TNBC patients than non-TNBC patients.[16] MDSCs are known to create an environment for tumor cells to utilize immune evasion by suppressing CD8$^+$ T-cells and expanding FOXP3$^+$ T-cells.[21,24] We also reported a decrease in MDSCs in the tumors of mice injected with TNBC cells with ΔNp63 inhibition, suggesting that ΔNp63$^+$ tumor cells had a role in the recruitment of MDSCs.[16] In the present study, we showed the effect of suppressing ΔNp63 on survival of MDSCs in established tumors in TNBC GEMMs as well as syngeneic TNBC models. Unlike xenografts of human tumor cells into immunodeficient mice, these models utilize immunocompetent mice, which are expected to mimic the immune cell response seen in human cancer patients. We found a decreased number of MDSCs, CD4$^+$ T-cells, and immune-suppressive FOXP3$^+$ T-cells and a concomitant increase in cytotoxic CD8$^+$ T-cells in *ΔNp63* cKO or inhibited tumors, suggesting remodeling from immune evasion to immune surveillance in established TNBC with ΔNp63 loss. These changes appear to be partly due to

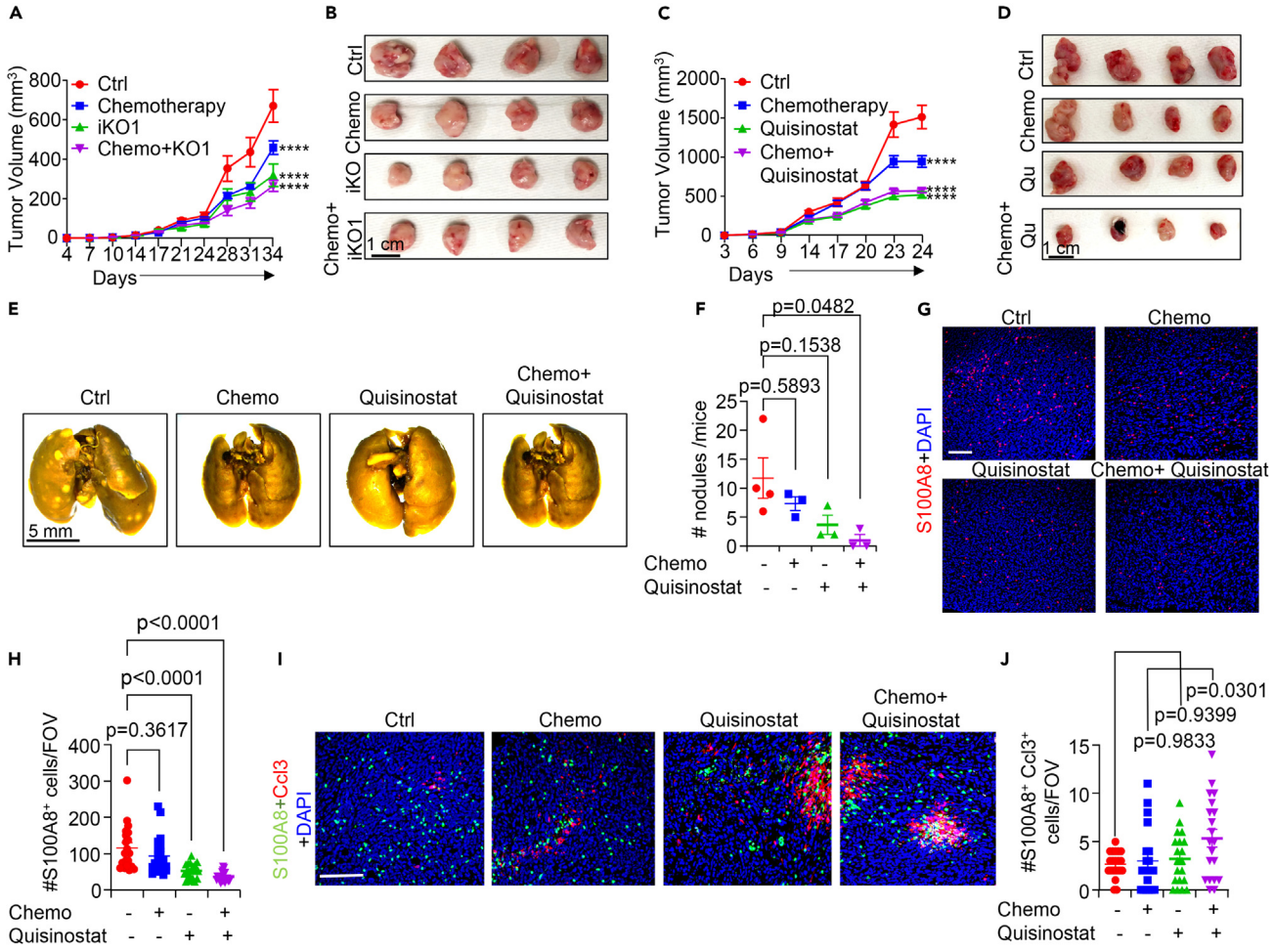

Figure 8. Combination of chemotherapy and targeting ΔNp63 decreased tumor proliferation

(A and B) 4T1 cells were injected into mammary fat pads of BALB/c mice and followed by injection of doxorubicin (Chemo) and doxycycline as food. Doxycycline was used to induce iKO of *ΔNp63*. Doxycycline alone (*ΔNp63* KO) and combination with doxorubicin (*ΔNp63* KO + Chemo) showed significant reduction in tumor growth compared to control (PBS only). n = 6 control, 6 Chemo, 4 iKO1, 8 Chemo+iKO1.

(C and D) 4T1 cells were injected into mammary fat pads of BALB/c mice. Mice were injected with doxorubicin (chemo) and HDACi Quisinostat. Treatment of Quisinostat alone or combination with doxorubicin decreased tumor growth significantly compared to control (PBS only) or doxorubicin. n = 4 control, n = 6 Chemo, n = 4 Quisinostat, n = 6 Chemo+Quisinostat.

(E and F) Analysis of metastatic lung nodules revealed that treatment of Quisinostat alone or combination treatment with doxorubicin significantly decreased lung metastasis. n = 4 control, n = 3 Chemo, Quisinostat, and Chemo+Quisinostat.

(G and H) IF was performed on tumors with S100A8 (red) antibody. Chemotherapy and Quisinostat significantly decreased MDSCs compared to control (PBS only), which showed the lowest number in the combination group. n = 4 tumors/group.

(I and J) IF was performed with S100A8 (green) and cleaved caspase 3 (Ccl3, red) antibodies. Combination therapy significantly increased $Ccl3^+$ MDSCs (yellow) compared to control (PBS only). n = 4 tumors/group. For all IF images, 20 random fields of view (FOVs) were chosen from 4 tumors/group. p values were calculated using two-way ANOVA with Bonferroni post-test adjustment (A, C) and one-way ANOVA with Tukey's multiple-comparisons *post hoc* test (F, H, J). ****p < 0.0001. (A, C, F, H, J) Data are presented as the mean ± SEM. Scale bars, 1 cm (B, D) and 5 mm (E) and 100 μm (G, I).

increased survival of MDSC by TNF-α. TNF-α is known to be involved in the survival of MDSC through TNFR2.[43] Our results are in line with previous reports and suggest the possibility that ΔNp63 promotes MDSC survival by participating in the TNF-α pathway. In particular, the level of TNF-α cytokine is responsible for MDSC survival compared to the receptors (TNFR1 and TNFR2) in TNBC. Furthermore, we found that decreased MDSC infiltration in ΔNp63-reduced tumors is associated with increased apoptosis of MDSCs. ΔNp63-inhibited tumor-bearing mice also showed decreased circulation of PMN-MDSC precursors, suggesting that inducing apoptosis of MDSCs in primary tumors can be connected to reductions in metastasis. RNA-seq data indicated that altered lipid metabolism in MDSCs is highly correlated with decreased survival and function of MDSCs. Altered lipid in MDSCs was confirmed with BODIPY staining, implying that $\Delta Np63^+$ tumor cells regulate lipid metabolism of MDSCs in a paracrine manner. Future studies will delineate the mechanistic function of altered metabolism of MDSC in TNBC.

It was reported that HDACi suppresses tumors in a ΔNp63-dependent manner.[34] There are 18 HDAC isoforms, and they can be targeted by isoform-selective HDACi as well as pan-HDACi.[46] Since most HDAC isoforms are involved in tumorigenesis, pan-HDACi acting polypharmacologically may be more effective than isoform-specific inhibitors.[47] In this study, we identified that Quisinostat, a second-generation pan-HDACi with improved efficacy,[35] was effective in ΔNp63-dependent manner in TNBC. Quisinostat appears to regulate the level of ΔNp63 protein by increasing FBWX7 protein, which is involved in the degradation of ΔNp63 protein, supporting previous findings.[34] Our data showed that Quisinostat suppressed tumor progression and metastasis by reshaping the immunosuppressive immune landscape. To date, five HDACis have been approved by the Food and Drug Administration (FDA) and have been successful in hematological neoplasms.[48] Drug repurposing, which develops a different use of an FDA-approved drug, is in the limelight because it costs less and takes less time than conventional new drug development.[49] Our results demonstrate the potential for drug repurposing of a new HDACi Quisinostat to treat ΔNp63^{+} TNBC.

In conclusion, targeting ΔNp63 in developed tumors indicates that ΔNp63 is crucial in tumor promotion, progression, and metastasis of TNBC. Of note, inhibiting ΔNp63^{+} tumor cells can interfere with control of MDSC survival. *ΔNp63* KO (icKO and iKO) tumors have a decreased number of MDSCs with compromised immunosuppressive activity which reshaped the immune landscape with increased cytotoxic T-cells. In addition, our data demonstrated that inhibition of ΔNp63 sensitized TNBC cells to chemotherapy. We propose that ΔNp63 is a potential therapeutic target for sensitizing metastatic stage IV TNBC patients with high MDSC number to chemotherapy.

Limitation of the study

Although we demonstrated *in vivo* that targeting ΔNp63 sensitizes TNBC to chemotherapy, these results are based on pre-clinical studies and therefore Quisinostat requires more rigorous validation in clinical studies. In addition, our RNA-seq and experimental results showed that TNF-α is deeply involved in the survival of MDSC, but these mechanisms deserve further investigation.

STAR★METHODS

Detailed methods are provided in the online version of this paper and include the following:

- KEY RESOURCES TABLE
- RESOURCE AVAILABILITY
  - Lead contact
  - Materials availability
  - Data and code availability
- EXPERIMENTAL MODEL AND STUDY PARTICIPANT DETAILS
  - Animal studies
- METHOD DETAILS
  - Knockout of cells
  - Overexpression *ΔNp63*
  - Western blot
  - Histological analysis, immunohistochemistry (IHC), and immunofluorescence (IF)
  - Flow analysis
  - RNA-seq analysis and gene set enrichment analysis (GSEA)
  - BODIPY staining
- QUANTIFICATION AND STATISTICAL ANALYSIS

SUPPLEMENTAL INFORMATION

Supplemental information can be found online at https://doi.org/10.1016/j.isci.2024.109366.

ACKNOWLEDGMENTS

We thank Dr. Pierre Chambon for *iK14-Cre* mice. We thank Dr. Elsa Flores for *ΔNp63*$^{f/f}$ mice. The authors thank the Penn Vet Comparative Pathology Core, Children's Hospital of Philadelphia (CHOP) histology core, Perelman School of Medicine histology core, and Cancer Modeling Shared Resource at the Sylvester Comprehensive Cancer Center of University of Miami (SCCC-UM) for their assistance with embedding and sectioning of tumor samples. We thank the members of the Flow Cytometry Core at the CHOP, the University of Pennsylvania, and the Flow Cytometry Shared Resource at SCCC-UM. We also thank Novogene Corporation Inc. for bulk mRNA-seq and analyses. This work was supported by grant from NCI-R01 (R01CA237243) grant to R.C.

AUTHOR CONTRIBUTIONS

R.C. designed all the experiments. U.K., R.D., and J.E.M. performed all the experiments. U.K. and R.C. wrote the manuscript. J.R. and M.A.B. constructed sgRNAs, made corresponding lentivirus, and provided technical advice on knockdown and knockout experiments. S.S.

constructed the mutant ΔNp63 and advised on design of experiments and interpretation of data. All authors discussed the results and commented on the manuscript.

DECLARATION OF INTERESTS

The authors declare no competing interests.

Received: July 17, 2023
Revised: December 20, 2023
Accepted: February 26, 2024
Published: February 29, 2024

REFERENCES

1. Rakha, E.A., El-Sayed, M.E., Green, A.R., Lee, A.H.S., Robertson, J.F., and Ellis, I.O. (2007). Prognostic markers in triple-negative breast cancer. Cancer *109*, 25–32.
2. Griffiths, C.L., and Olin, J.L. (2012). Triple negative breast cancer: a brief review of its characteristics and treatment options. J. Pharm. Pract. *25*, 319–323.
3. Nitiss, K.C., and Nitiss, J.L. (2014). Twisting and Ironing: Doxorubicin Cardiotoxicity by Mitochondrial DNA DamageDoxorubicin Targets Mitochondrial DNA. Clin. Cancer Res. *20*, 4737–4739.
4. Turton, N.J., Judah, D.J., Riley, J., Davies, R., Lipson, D., Styles, J.A., Smith, A.G., and Gant, T.W. (2001). Gene expression and amplification in breast carcinoma cells with intrinsic and acquired doxorubicin resistance. Oncogene *20*, 1300–1306.
5. Li, Y., Zhang, H., Merkher, Y., Chen, L., Liu, N., Leonov, S., and Chen, Y. (2022). Recent advances in therapeutic strategies for triple-negative breast cancer. J. Hematol. Oncol. *15*, 121.
6. Hallett, R.M., Dvorkin-Gheva, A., Bane, A., and Hassell, J.A. (2012). A gene signature for predicting outcome in patients with basal-like breast cancer. Sci. Rep. *2*, 227.
7. Crum, C.P., and McKeon, F.D. (2010). p63 in epithelial survival, germ cell surveillance, and neoplasia. Annu. Rev. Pathol. *5*, 349–371.
8. Mills, A.A., Zheng, B., Wang, X.-J., Vogel, H., Roop, D.R., and Bradley, A. (1999). p63 is a p53 homologue required for limb and epidermal morphogenesis. Nature *398*, 708–713.
9. Yang, A., Kaghad, M., Wang, Y., Gillett, E., Fleming, M.D., Dötsch, V., Andrews, N.C., Caput, D., and McKeon, F. (1998). p63, a p53 homolog at 3q27–29, encodes multiple products with transactivating, death-inducing, and dominant-negative activities. Mol. Cell *2*, 305–316.
10. Guo, X., Keyes, W.M., Papazoglu, C., Zuber, J., Li, W., Lowe, S.W., Vogel, H., and Mills, A.A. (2009). TAp63 induces senescence and suppresses tumorigenesis in vivo. Nat. Cell Biol. *11*, 1451–1457.
11. Flores, E.R., Tsai, K.Y., Crowley, D., Sengupta, S., Yang, A., McKeon, F., and Jacks, T. (2002). p63 and p73 are required for p53-dependent apoptosis in response to DNA damage. Nature *416*, 560–564.
12. Saladi, S.V., Ross, K., Karaayvaz, M., Tata, P.R., Mou, H., Rajagopal, J., Ramaswamy, S., and Ellisen, L.W. (2017). ACTL6A is co-amplified with p63 in squamous cell carcinoma to drive YAP activation, regenerative proliferation, and poor prognosis. Cancer Cell *31*, 35–49.
13. Glathar, A.R., Oyelakin, A., Gluck, C., Bard, J., and Sinha, S. (2022). p63 Directs Subtype-Specific Gene Expression in HPV+ Head and Neck Squamous Cell Carcinoma. Front. Oncol. *12*, 879054.
14. Rocco, J.W., Leong, C.-O., Kuperwasser, N., DeYoung, M.P., and Ellisen, L.W. (2006). p63 mediates survival in squamous cell carcinoma by suppression of p73-dependent apoptosis. Cancer Cell *9*, 45–56.
15. Di Giacomo, V., Tian, T.V., Mas, A., Pecoraro, M., Batlle-Morera, L., Noya, L., Martín-Caballero, J., Ruberte, J., and Keyes, W.M. (2017). ΔNp63α promotes adhesion of metastatic prostate cancer cells to the bone through regulation of CD82. Oncogene *36*, 4381–4392.
16. Kumar, S., Wilkes, D.W., Samuel, N., Blanco, M.A., Nayak, A., Alicea-Torres, K., Gluck, C., Sinha, S., Gabrilovich, D., and Chakrabarti, R. (2018). ΔNp63-driven recruitment of myeloid-derived suppressor cells promotes metastasis in triple-negative breast cancer. J. Clin. Invest. *128*, 5095–5109.
17. Chakrabarti, R., Wei, Y., Hwang, J., Hang, X., Andres Blanco, M., Choudhury, A., Tiede, B., Romano, R.-A., DeCoste, C., Mercatali, L., et al. (2014). ΔNp63 promotes stem cell activity in mammary gland development and basal-like breast cancer by enhancing Fzd7 expression and Wnt signalling. Nat. Cell Biol. *16*, 1004–1013.
18. Leong, C.-O., Vidnovic, N., DeYoung, M.P., Sgroi, D., and Ellisen, L.W. (2007). The p63/p73 network mediates chemosensitivity to cisplatin in a biologically defined subset of primary breast cancers. J. Clin. Invest. *117*, 1370–1380.
19. Marvel, D., and Gabrilovich, D.I. (2015). Myeloid-derived suppressor cells in the tumor microenvironment: expect the unexpected. J. Clin. Invest. *125*, 3356–3364.
20. Veglia, F., Sanseviero, E., and Gabrilovich, D.I. (2021). Myeloid-derived suppressor cells in the era of increasing myeloid cell diversity. Nat. Rev. Immunol. *21*, 485–498.
21. Yang, Z., Guo, J., Weng, L., Tang, W., Jin, S., and Ma, W. (2020). Myeloid-derived suppressor cells—new and exciting players in lung cancer. J. Hematol. Oncol. *13*, 10–17.
22. Lindau, D., Gielen, P., Kroesen, M., Wesseling, P., and Adema, G.J. (2013). The immunosuppressive tumour network: myeloid-derived suppressor cells, regulatory T cells and natural killer T cells. Immunology *138*, 105–115.
23. Ostrand-Rosenberg, S., Sinha, P., Beury, D.W., and Clements, V.K. (2012). Cross-talk between myeloid-derived suppressor cells (MDSC), macrophages, and dendritic cells enhances tumor-induced immune suppression. Semin. Cancer Biol. *4*, 275–281.
24. Gabrilovich, D.I., and Nagaraj, S. (2009). Myeloid-derived suppressor cells as regulators of the immune system. Nat. Rev. Immunol. *9*, 162–174.
25. Li, Y., Hively, W.P., and Varmus, H.E. (2000). Use of MMTV-Wnt-1 transgenic mice for studying the genetic basis of breast cancer. Oncogene *19*, 1002–1009.
26. Pfefferle, A.D., Herschkowitz, J.I., Usary, J., Harrell, J.C., Spike, B.T., Adams, J.R., Torres-Arzayus, M.I., Brown, M., Egan, S.E., Wahl, G.M., et al. (2013). Transcriptomic classification of genetically engineered mouse models of breast cancer identifies human subtype counterparts. Genome Biol. *14*, R125.
27. Li, M., Indra, A.K., Warot, X., Brocard, J., Messaddeq, N., Kato, S., Metzger, D., and Chambon, P. (2000). Skin abnormalities generated by temporally controlled RXRα mutations in mouse epidermis. Nature *407*, 633–636.
28. Indra, A.K., Li, M., Brocard, J., Warot, X., Bornert, J.-M., Gérard, C., Messaddeq, N., Chambon, P., and Metzger, D. (2000). Targeted somatic mutagenesis in mouse epidermis. Horm. Res. *54*, 296–300.
29. Chakravarti, D., Su, X., Cho, M.S., Bui, N.H.B., Coarfa, C., Venkatanarayan, A., Benham, A.L., Flores González, R.E., Alana, J., Xiao, W., et al. (2014). Induced multipotency in adult keratinocytes through down-regulation of ΔNp63 or DGCR8. Proc. Natl. Acad. Sci. USA *111*, E572–E581.
30. Kumar, S., Nandi, A., Mahesh, A., Sinha, S., Flores, E., and Chakrabarti, R. (2020). Inducible knockout ofΔ Np63 alters cell polarity and metabolism during pubertal mammary gland development. FEBS Lett. *594*, 973–985.
31. Gatti-Mays, M.E., Balko, J.M., Gameiro, S.R., Bear, H.D., Prabhakaran, S., Fukui, J., Disis, M.L., Nanda, R., Gulley, J.L., Kalinsky, K., et al. (2019). If we build it they will come: targeting the immune response to breast cancer. NPJ breast cancer *5*, 37.
32. Wang, T., Wei, J.J., Sabatini, D.M., and Lander, E.S. (2014). Genetic screens in human cells using the CRISPR-Cas9 system. Science *343*, 80–84.
33. Pulaski, B.A., and Ostrand-Rosenberg, S. (2000). Mouse 4T1 breast tumor model. Curr. Protoc. Immunol. *39*, 20–22.
34. Napoli, M., Venkatanarayan, A., Raulji, P., Meyers, B.A., Norton, W., Mangala, L.S., Sood, A.K., Rodriguez-Aguayo, C., Lopez-Berestein, G., Vin, H., et al. (2016). ΔNp63/DGCR8-dependent microRNAs mediate

therapeutic efficacy of HDAC inhibitors in cancer. Cancer Cell *29*, 874–888.

35. He, B., Dai, L., Zhang, X., Chen, D., Wu, J., Feng, X., Zhang, Y., Xie, H., Zhou, L., Wu, J., and Zheng, S. (2018). The HDAC inhibitor quisinostat (JNJ-26481585) supresses hepatocellular carcinoma alone and synergistically in combination with sorafenib by G0/G1 phase arrest and apoptosis induction. Int. J. Biol. Sci. *14*, 1845–1858.
36. Galli, F., Rossi, M., D'Alessandra, Y., De Simone, M., Lopardo, T., Haupt, Y., Alsheich-Bartok, O., Anzi, S., Shaulian, E., Calabrò, V., et al. (2010). MDM2 and Fbw7 cooperate to induce p63 protein degradation following DNA damage and cell differentiation. J. Cell Sci. *123*, 2423–2433.
37. Aprelikova, O., Tomlinson, C.C., Hoenerhoff, M., Hixon, J.A., Durum, S.K., Qiu, T.-h., He, S., Burkett, S., Liu, Z.-Y., Swanson, S.M., and Green, J.E. (2016). Development and preclinical application of an immunocompetent transplant model of basal breast cancer with lung, liver and brain metastases. PLoS One *11*, e0155262.
38. Singh, S., Kumar, S., Srivastava, R.K., Nandi, A., Thacker, G., Murali, H., Kim, S., Baldeon, M., Tobias, J., Blanco, M.A., et al. (2020). Loss of ELF5–FBXW7 stabilizes IFNGR1 to promote the growth and metastasis of triple-negative breast cancer through interferon-γ signalling. Nat. Cell Biol. *22*, 591–602.
39. Wu, H., Weidinger, C., Schmidt, F., Keye, J., Friedrich, M., Yerinde, C., Willimsky, G., Qin, Z., Siegmund, B., and Glauben, R. (2017). Oleate but not stearate induces the regulatory phenotype of myeloid suppressor cells. Sci. Rep. *7*, 7498.
40. Veglia, F., Tyurin, V.A., Blasi, M., De Leo, A., Kossenkov, A.V., Donthireddy, L., To, T.K.J., Schug, Z., Basu, S., Wang, F., et al. (2019). Fatty acid transport protein 2 reprograms neutrophils in cancer. Nature *569*, 73–78.
41. Yan, D., Adeshakin, A.O., Xu, M., Afolabi, L.O., Zhang, G., Chen, Y.H., and Wan, X. (2019). Lipid metabolic pathways confer the immunosuppressive function of myeloid-derived suppressor cells in tumor. Front. Immunol. *10*, 1399.
42. Aarts, C.E.M., Hiemstra, I.H., Béguin, E.P., Hoogendijk, A.J., Bouchmal, S., van Houdt, M., Tool, A.T.J., Mul, E., Jansen, M.H., Janssen, H., et al. (2019). Activated neutrophils exert myeloid-derived suppressor cell activity damaging T cells beyond repair. Blood Adv. *3*, 3562–3574.
43. Zhao, X., Rong, L., Zhao, X., Li, X., Liu, X., Deng, J., Wu, H., Xu, X., Erben, U., Wu, P., et al. (2012). TNF signaling drives myeloid-derived suppressor cell accumulation. J. Clin. Invest. *122*, 4094–4104.
44. Nedeljković, M., and Damjanović, A. (2019). Mechanisms of chemotherapy resistance in triple-negative breast cancer—how we can rise to the challenge. Cells *8*, 957.
45. Mortezaee, K. (2020). Immune escape: A critical hallmark in solid tumors. Life Sci. *258*, 118110.
46. Li, Y., and Seto, E. (2016). HDACs and HDAC inhibitors in cancer development and therapy. Cold Spring Harb. Perspect. Med. *6*, a026831.
47. de Lera, A.R., and Ganesan, A. (2016). Epigenetic polypharmacology: from combination therapy to multitargeted drugs. Clin. Epigenetics *8*, 105–121.
48. Shanmugam, G., Rakshit, S., and Sarkar, K. (2022). HDAC inhibitors: Targets for tumor therapy, immune modulation and lung diseases. Transl. Oncol. *16*, 101312.
49. Pushpakom, S., Iorio, F., Eyers, P.A., Escott, K.J., Hopper, S., Wells, A., Doig, A., Guilliams, T., Latimer, J., McNamee, C., et al. (2019). Drug repurposing: progress, challenges and recommendations. Nat. Rev. Drug Discov. *18*, 41–58.
50. Romano, R.-A., Birkaya, B., and Sinha, S. (2007). A functional enhancer of keratin14 is a direct transcriptional target of ΔNp63. J. Invest. Dermatol. *127*, 1175–1186.
51. Chakrabarti, R., Hwang, J., Andres Blanco, M., Wei, Y., Lukačišin, M., Romano, R.-A., Smalley, K., Liu, S., Yang, Q., Ibrahim, T., et al. (2012). Elf5 inhibits the epithelial–mesenchymal transition in mammary gland development and breast cancer metastasis by transcriptionally repressing Snail2. Nat. Cell Biol. *14*, 1212–1222.
52. Thacker, G., Henry, S., Nandi, A., Debnath, R., Singh, S., Nayak, A., Susnik, B., Boone, M.M., Zhang, Q., Kesmodel, S.B., et al. (2023). Immature natural killer cells promote progression of triple-negative breast cancer. Sci. Transl. Med. *15*, eabl4414.
53. Nandi, A., Debnath, R., Nayak, A., To, T.K.J., Thacker, G., Reilly, M., Gumber, S., Karagounis, I., Li, N., Lengner, C.J., et al. (2022). Dll1-mediated notch signaling drives tumor cell cross-talk with cancer-associated fibroblasts to promote radioresistance in breast cancer. Cancer Res. *82*, 3718–3733.

STAR★METHODS

KEY RESOURCES TABLE

REAGENT or RESOURCE	SOURCE	IDENTIFIER
Antibodies		
Anti-ΔNp63 Antibody (4A4 clone)	Laboratory of Dr. Rumela Chakrabarti, similar to P3737 of Sigma	N/A
Anti-FBXW7 Antibody	Thermo Fisher Scientific	Cat#A301-721A; RRID:AB_1210898
Anti-β-actin Antibody	Sigma-Aldrich	Cat#A5441; RRID:AB_476744
Anti-CD4 Antibody	CST	Cat#25229S; RRID:AB_2798898
Anti-CD8 Antibody	CST	Cat#98941S; RRID:AB_2756376
Anti-FOXP3 Antibody	CST	Cat#12653s; RRID:AB_2797979
Anti-Ki67 Antibody	CST	Cat#12202S; AB_2620142
Anti-Cleaved caspase 3 Antibody	CST	Cat#9661S; RRID:AB_2341188
Anti-S100A8 Antibody	R&D Systems	Cat#MAB3059; RRID:AB_2184252
Anti-K14 Antibody	Biolegend	Cat#905301; RRID:AB_2565048
PE/Cy7 Anti-CD45 Antibody	BD Biosciences	Cat#552848; RRID:AB_394489
BV421 Anti-CD45 Antibody	BD Biosciences	Cat#563890; RRID:AB_2651151
PerCP/Cy5.5 Anti-CD11b Antibody	BD Biosciences	Cat#550993; RRID:AB_394002
APC/Cy7 Anti-Gr1 Antibody	BD Biosciences	Cat#557661; RRID:AB_396775
APC Anti-Ly6C Antibody	BD Biosciences	Cat#560595; RRID:AB_1727554
PE Anti-Ly6G Antibody	StemCell	Cat#60031PE; RRID:AB_2877150
PerCP/Cy5.5 Anti-CD3 Antibody	Biolegend	Cat#100218; RRID:AB_1595492
APC/Cy7 Anti-CD4 Antibody	BD Biosciences	Cat#552051; RRID:AB_394331
PE/Cy7 Anti-CD8 Antibody	BD Biosciences	Cat#552877; RRID:AB_394506
PE Anti-Cleaved caspase 3 Antibody	BD Biosciences	Cat#550821; RRID:AB_393906
APC Anti-EpCAM Antibody	Biolegend	Cat#118213; RRID:AB_1134102
APC Anti-CD11c Antibody	BD Biosciences	Cat#550261; RRID:AB_398460
BV605 Anti-F4/80 Antibody	Biolegend	Cat#123133; RRID:AB_2562305
PE Anti-TNF-α Antibody	Thermo Fisher Scientific	Cat#12-7321-81; RRID:AB_466198
Bacterial and virus strains		
NEB® Stable Competent E. coli (High Efficiency)	New England Biolabs	Cat#C3040H
Chemicals, peptides, and recombinant proteins		
CD326 (EpCAM) MicroBeads, mouse	Miltenyi Biotec	Cat#130-105-958; RRID:AB_2936423
BD IMag™ Anti-Mouse Ly-6G and Ly-6C Particles	BD Biosciences	Cat#558111; RRID:AB_398656
Quisinostat	Selleckchem	Cat#S1096
Doxorubicin	LC laboratories	Cat#D4000
Tamoxifen	Sigma-Aldrich	Cat#T5648
DMEM	Thermo Fisher Scientific	Cat#11960-051
FBS	GeminiBio	Cat#900-108
Penicillin/Streptomycin	Thermo Fisher Scientific	Cat#15140-122
Insulin	Sigma-Aldrich	Cat#I9278
Polybrene	Sigma-Aldrich	Cat#H9268
Puromycin	Sigma-Aldrich	Cat#P8833
Hygromycin	Thermo Fisher Scientific	Cat#10687-010
Doxycycline Rodent Diet	Bio-Serv	Cat#S3888

(*Continued on next page*)

Continued

REAGENT or RESOURCE	SOURCE	IDENTIFIER
ECL solutions	Thermo Fisher Scientific	Cat#34096
Collagenase from *Clostridium histolyticum*	Sigma–Aldrich	Cat#C2674
Hyaluronidase	Sigma–Aldrich	Cat#H3884
DMEM/F-12	Thermo Fisher Scientific	Cat#11330-032
Gentamicin	Thermo Fisher Scientific	Cat#15750-060
Cholera toxin from *Vibrio cholerae*	Sigma-Aldrich	Cat#C8052
Hydrocortisone	Sigma–Aldrich	Cat#H0888
Trypsin-EDTA	Thermo Fisher Scientific	Cat#25200-056
Dispase	Thermo Fisher Scientific	Cat#100-10-023
DNAse I	Sigma–Aldrich	Cat#D5025
Fetal calf serum	GeminiBio	Cat#100-504
Ammonium chloride	Calbiochem	168320
Recombinant Human Epidermal Growth Factor/EGF	Novoprotein	Cat#C029
BODIPY	Thermo Fisher Scientific	Cat#D3922
Fixation/Permeabilization Solution	BD Biosciences	Cat#554722
PageRuler™ Prestained Protein Ladder, 10 to 180 kDa	Thermo Fisher Scientific	Cat#26616
Critical commercial assays		
Purelink RNA mini kit	Thermo Fisher Scientific	Cat#12183018A
SuperScript™ IV First-Strand Synthesis System	Thermo Fisher Scientific	Cat#18091050
Power SYBR™ Green PCR Master Mix	Thermo Fisher Scientific	Cat#4367659
Deposited data		
4T1; control MDSC vs. 4T1; *ΔNp63* iKO1 MDSC-RNA-sequencing data	This manuscript	GEO: GSE PRJNA1053819
HCC1806; Ctrl vs. *ΔNp63* KD	Kumar et al.[16]	GEO: GSE102377
Experimental models: Cell lines		
Mouse: 4T1/LIG Murine TNBC cells	Laboratory of Dr. Yibin Kang	N/A
Human: HEK293T Human kidney cells	ATCC	Cat#CRL-3216; RRID:CVCL_0063
Experimental models: Organisms/strains		
Mouse: BALB/c *Mus musculus*	The Jackson Laboratory	Cat#000651; RRID:IMSR_JAX:000651
Mouse: C3-T^{Het} *Mus musculus*	Laboratory of Dr. Rumela Chakrabarti	N/A
Mouse: C3(1)/Tag-REAR *Mus musculus*	The Jackson Laboratory	Cat#030386; RRID:IMSR_JAX:030386
Mouse: MMTV-Wnt1 *Mus musculus*	The Jackson Laboratory	Cat#002870; RRID:IMSR_JAX:002870
Mouse: iK14-Cre *Mus musculus*	Laboratory of Dr. Pierre Chambon	N/A
Mouse: *ΔNp63*$^{f/f}$ *Mus musculus*	Laboratory of Dr. Elsa Flores	N/A
Oligonucleotides		
Primer: *ΔNp63* Forward: TGCCCAGACTCAATTTAGTGA	This paper	N/A
Primer: *ΔNp63* Reverse: GAGGAGCCGTCCTGAATCTG	This paper	N/A
Primer: *Gapdh* Forward: TTCCACTCTTCCACCTTCGATGC	This paper	N/A
Primer: *Gapdh* Reverse: GGGTCTGGGATGGAAATTGTGAGG	This paper	N/A
Primer: *Tnfr1* Forward: GCTGTTGCCCCTGGTTATCT	This paper	N/A
Primer: *Tnfr1* Reverse: ATGGAGTAGACTTCGGGCCT	This paper	N/A

(*Continued on next page*)

Continued

REAGENT or RESOURCE	SOURCE	IDENTIFIER
Primer: *Tnfr2* Forward: CCAGCTTAGGGCTCTGCAAT	This paper	N/A
Primer: *Tnfr2* Reverse: GATTCTGGACTGCCCATCCT	This paper	N/A
Recombinant DNA		
Plasmid: pCMV-VSV-G	Addgene	RRID:Addgene_8454
Plasmid: pCMV-dR8.2 dvpr	Addgene	RRID:Addgene_8455
Plasmid: pCW-Cas9	Laboratory of Dr. Mario Andrés Blanco	RRID:Addgene_50661
Plasmid: lentiGuide-Hygro-dTomato	Laboratory of Dr. Mario Andrés Blanco	RRID:Addgene_99376
Plasmid: lentiGuide-Hygro-dTomato targeting Murine *ΔNp63*: *ΔNp63* gRNA #1:CTTAGAAGATTCGCAGCGCA *ΔNp63* gRNA #2:GTTAGCAGTGAGACTGGTCA	This manuscript	N/A
Plasmid: lentiORF pLEX-MCS	Laboratory of Dr. Satrajit Sinha	Cat#OHS4735
Plasmid: lentiORF pLEX-Murine WT *ΔNp63*	Laboratory of Dr. Satrajit Sinha	N/A
Plasmid: lentiORF pLEX-Murine R304W *ΔNp63*	Laboratory of Dr. Satrajit Sinha	N/A
Software and algorithms		
FlowJo v10	www.flowjo.com	http://docs.flowjo.com/
GraphPad Prism 9	GraphPad Software	https://www.graphpad.com/scientific-software/prism/

RESOURCE AVAILABILITY

Lead contact

Further information and requests for resources and reagents should be directed to and will be fulfilled by the Lead Contact, Rumela Chakrabarti (rxc1335@miami.edu).

Materials availability

- Further information and requests for mouse lines generated in this study will be available upon reasonable request to the lead contact.

Data and code availability

- The transcriptomic data for MDSC and HCC1806 samples is publicly available from Gene Expression Omnibus (https://www.ncbi.nlm.nih.gov/geo/).
- No original code was generated in this paper.
- Any additional information required to reanalyze the data reported in this paper is available from the lead contact upon request.

EXPERIMENTAL MODEL AND STUDY PARTICIPANT DETAILS

Animal studies

Animal procedures were performed in accordance with the Institutional Animal Care and Use Committee (IACUC) of the University of Pennsylvania and the University of Miami. C3(1)/Tag (C3-T); *Elf5*$^{+/-}$ (^{Het}) FVB mice have been previously described.[38] Mice were genotyped with C3 primers and LacZ primers for knock-in of Elf5$^{+/-}$. REAR mice were obtained from Jackson Laboratories and genotyping was performed according to company protocols. For mammary fat pads tumor models, 4–5 weeks old female mice (Rear or BALB/c) were injected with tumor cells (C3-T^{Het} or 4T1 cells) into the mammary fat pads. The harvested C3-T^{Het} tumor was isolated into single cells (Please see Flow analysis method). Isolated single cells from C3-T^{Het} tumor were enriched for EpCAM^{+} tumor cells by using commercial kits (Miltenyi Biotec; 130-105-958) and followed by mammary fat pads injection. All mammary fat pads tumors were palpated twice a week. 40 mg/kg HDACi, Quisinostat (Selleckchem; S1096), and 2 mg/kg doxorubicin (LC laboratories; D4000) were administered intraperitoneally every other day and twice a week, respectively, when the tumor size reached 65 mm^3. To evaluate lung metastasis, 4T1 cells were injected into the tail vein of BALB/c mice. For TNBC GEMM with icKO of *ΔNp63*, we used *MMTV-Wnt1;iK14-Cre;ΔNp63*$^{f/f}$ mice. *iK14-Cre* mice have a tamoxifen-inducible iK14 promoter, which can induce expression of Cre in both basal and luminal epithelium. *iK14-Cre* mice were crossed with *ΔNp63*$^{f/f}$ mice and sequentially crossed with MMTV-Wnt1 mice. MMTV-Wnt1 mice with MMTV LTR as enhancer, Wnt1 promoter and Wnt1 gene were used to study spontaneous TNBC. Female mice were used. When the tumor was palpable, we intraperitoneally injected 70 μg/mouse/day of tamoxifen (Sigma-Aldrich; T5648) to induce cKO of *ΔNp63* for 3 days. Tumor size was monitored for 1 week following tamoxifen treatment.

METHOD DETAILS

Knockout of cells

4T1 cells were cultured in DMEM (Gibco, 11960-051) supplemented with 10% FBS (GeminiBio; 900-108), 1% penicillin/streptomycin (Gibco; 15140-122) and insulin (10 μg/mL; Sigma-Aldrich; I9278). Lentivirus was packaged with 1 μg pCMV-VSV-G (Addgene; 8454), 2.5 μg pCMV-dR8.2 dvpr (Addgene; 8455) and 4 μg target DNA using HEK293T cells. Next day, the media was changed to complete DMEM media. The supernatant was collected twice after 48 h and 72 h of transfection, spun down to remove floating cells and filtered by using 0.45 μm syringe filter (Fisherbrand; 09-719D). For lentiviral infection, 1 μg/mL polybrene (Sigma-Aldrich; H9268) was supplemented in virus-containing supernatant. 4T1 cells were infected with lentivirus carrying doxycycline-inducible pCW-Cas9 (Addgene; 50661) and selected with 0.5 μg/mL puromycin (Sigma-Aldrich; P8833). After 5–7 days of selection, cells were sequentially infected with lentivirus carrying lentiGuide-Hygro-dTomato (Addgene; 99376) targeting mouse *ΔNp63* and followed by selection with 0.5 μg/mL puromycin and 20 μg/mL hygromycin (Gibco; 10687-010) for 7 days. The targeting sgRNA sequence for mouse *ΔNp63* KO1 and KO2 are 5′-CTTAGAAGATTCGCAGCGCA-3′ and 5′-GTTAGCAGTGAGACTGGTCA-3′, respectively. The cells were injected into the mammary fat pads or tail vein in 4–5 weeks old female BALB/c mice. The mice were fed with Doxycycline Rodent Diet (Bio-Serv, S3888) to establish iKO of *ΔNp63* after tumor were 3 × 3 mm.

Overexpression *ΔNp63*

4T1 cells were infected with lentivirus carrying *ΔNp63* or R304W *ΔNp63* with mutation in the DNA binding domain (ΔNp63-mt). The mouse WT *ΔNp63* and mutant *ΔNp63* cDNAs was excised from the pCMV-HA plasmids and are described before[50] and sub-cloned into BamH1-Not1 sites in the pLEX-MCS vector (Open Biosystems; OHS4735).

Western blot

Whole-cell extracts from cell lines and tumors were prepared as previously described.[51] Proteins were resolved by SDS-PAGE, transferred to PVDF membranes (Millipore; IPVH00010) and analyzed using the specified antibodies and ECL solutions (Thermo Scientific; 34096). Details of antibodies are described in Table S1.

Histological analysis, immunohistochemistry (IHC), and immunofluorescence (IF)

For histological analysis, mouse tissue was processed as previously described.[51] Slides were counterstained with hematoxylin for IHC and nuclei were counterstained with DAPI for IF. Images of tissues were taken using a Leica DMi8 and Nikon TiE. Scoring was performed for multiple fields of view (FOV) per sample. Details of antibodies are described in Table S1.

Flow analysis

A single-cell suspension for tumor flow analysis was prepared as previously described.[17] Briefly, the tumor was minced and digested with collagenase from *Clostridium histolyticum* (300 units/ml; Sigma–Aldrich; C2674) and hyaluronidase (100 units/ml; Sigma–Aldrich; H3884) in DMEM/F-12 (Gibco; 11330-032) supplemented with 5% fetal bovine serum (GeminiBio; 900-108), Gentamicin (50 μg/mL; Gibco; 15750-060), human epidermal growth factor (10 ng/mL; Novoprotein; C029), insulin (5 μg/mL; Sigma-Aldrich; I9278), cholera toxin from *Vibrio cholerae* (20 ng/mL; Sigma-Aldrich; C8052) and hydrocortisone (500 ng/mL; Sigma–Aldrich; H0888). After tissue digestion, tumor cells were isolated in single cells using 0.25% trypsin EDTA (Gibco; 25200-056) and Dispase/DNAse I solution (100 μg/mL DNAse I (Sigma–Aldrich; D5025) and 5 mg/mL dispase (Gibco; 17105-041) in PBS (Gibco; 100-10-023) sequentially. 5% fetal calf serum (GeminiBio; 100–504) and 50 μg/mL Gentamicin in PBS was added at each intermediate step to stop the enzyme reaction. Red blood cells were removed by incubation in 0.64% sterile ammonium chloride (Calbiochem; 168320) in Milli-Q water for 5 min at 37°C. Tumor cells were filtered through a 40-μm strainer (Greiner Bio-One; 542040) to obtain single cells. Blood was incubated with 0.64% sterile ammonium chloride to remove red blood cells. Cells were stained at room temperature in the dark for 30 min with the combination of different antibodies described in Tables S2 and S3. For TNF-α and Ccl3, the stained cells are fixed/permeabilized with Fixation/Permeabilization Solution (BD Biosciences; 554722). The fixed/permeabilized cells are stained with anti-TNF-α or anti-Ccl3 antibody. Because 4T1 tumor cells with *ΔNp63* OE expressed GFP, we couldn't run same FACS panels for EpCAM and TNF-α used for *ΔNp63* icKO tumors. Therefore, we enriched $EpCAM^+$ tumor cells with commercial anti-EpCAM antibody attached to microbeads (Miltenyi; 130-105-958). The enriched $EpCAM^+$ tumor cells were fixed/permeabilized and stained with anti-TNF-α antibody. An LSRII/Fortessa Flow Cytometer (BD Biosciences) and FlowJo software (Tree Star) was used for FACS analysis.

RNA-seq analysis and gene set enrichment analysis (GSEA)

RNA-seq was performed by Novogene following standard process.[52,53] RNA-seq was performed by DNA Link Inc. (Seoul, South Korea) according to the Kapa Biosystems Inc. (MA, USA) RNA-seq Library Quantification Kit protocol. Thirty million reads were obtained per sample and the data were deposited in NCBI's Gene Expression Omnibus (GEO) database with accession number GSE PRJNA1053819. For gene expression analysis, reads were aligned to the hg38 UCSC assembly with TopHat version 2.0.14 and Bowtie version 2.10. GFF file was obtained from the Genome Reference Consortium Human Build 38 patch release 9. The distribution of alignments was analyzed with Cufflinks version 2.2.1. FPM values were normalized. Differential expression testing was performed with Cuffdiff version 2.2.1, but FPKM values were calculated with Cufflinks. GSEA was performed using GSEA2.2.4 software to generate an enrichment score for gene sets in Hallmark C2.all, C5.all, and

C6.all with default settings. Gene sets were tested for enrichment in a rank-ordered list and enrichment scores were calculated with a weighted Kolmogorov-Smirnov-like statistic.

BODIPY staining

Cells were stained with 200 μL of 2 μM BODIPY (Invitrogen, D3922) in 37°C for 30 min. After 30 min of incubation, cells were washed and BODIPY was analyzed with the FITC channel. To analyze *ΔNp63* icKO tumor, cells are stained with antibody cocktails described in Tables S2 and S3 and followed with BODIPY staining. Because 4T1 tumor cells with *ΔNp63* OE expressed GFP, we couldn't run same FACS panels for BODIPY used for *ΔNp63* icKO tumors. Therefore, we enriched $Gr1^+$ MDSCs with commercial anti-Gr1 antibody attached to microbeads (BD Biosciences; 558111) before BODIPY staining.

QUANTIFICATION AND STATISTICAL ANALYSIS

The results were quantified using GraphPad Prism (version 9). The significance of differences was calculated using two-tailed Student's *t* test for normally distributed datasets with confidence intervals of 95%. The tumor growth datasets were analyzed using the two-way analysis of variance (ANOVA) to compute statistical significance. For parametric data with multiple comparisons, one-way ANOVA was used. Tukey's post hoc test for pairwise comparisons showed significant differences between each pair of groups.